Chapter 2.1b

Ferrar Large Igneous Province: petrology

David H. Elliot[1]*[2] and Thomas. H. Fleming[2]

[1]School of Earth Sciences and Byrd Polar and Climate Research Center, Ohio State University, Columbus, OH 43210, USA

[2]Department of Earth Sciences, Southern Connecticut State University, New Haven, CT 06515, USA

DHE, 0000-0002-6111-0508; THF, 0000-0001-7091-7699
*Correspondence: elliot.1@osu.edu

Abstract: The Lower Jurassic Ferrar Large Igneous Province consists predominantly of intrusive rocks, which crop out over a distance of 3500 km. In comparison, extrusive rocks are more restricted geographically. Geochemically, the province is divided into the Mount Fazio Chemical Type, forming more than 99% of the exposed province, and the Scarab Peak Chemical Type, which in the Ross Sea sector is restricted to the uppermost lava. The former exhibits a range of compositions (SiO_2 = 52–59%; MgO = 9.2–2.6%; Zr = 60–175 ppm; Sr_i = 0.7081–0.7138; ε_{Nd} = −6.0 to −3.8), whereas the latter has a restricted composition (SiO_2 = *c.* 58%; MgO = *c.* 2.3%; Zr = *c.* 230 ppm; Sr_i = 0.7090–0.7097; ε_{Nd} = −4.4 to −4.1). Both chemical types are characterized by enriched initial isotope compositions of neodymium and strontium, low abundances of high field strength elements, and crust-like trace element patterns. The most basic rocks, olivine-bearing dolerites, indicate that these geochemical characteristics were inherited from a mantle source modified by subduction processes, possibly the incorporation of sediment. In one model, magmas were derived from a linear source having multiple sites of generation each of which evolved to yield, in sum, the province-wide coherent geochemistry. The preferred interpretation is that the remarkably coherent geochemistry and short duration of emplacement demonstrate derivation from a single source inferred to have been located in the proto-Weddell Sea region. The spatial variation in geochemical characteristics of the lavas suggests distinct magma batches erupted at the surface, whereas no clear geographical pattern is evident for intrusive rocks.

An overview of the Ferrar Large Igneous Province (FLIP) is given in the introduction to the Ferrar LIP volcanology chapter in this Memoir (Elliot *et al.* 2021), and includes a summary of the existing age determinations. In brief, based on U–Pb zircon analyses, the duration of emplacement of the Ferrar Dolerite and Dufek intrusion is estimated to be 349 ± 0.49 kyr, with ages ranging from 182.78 ± 0.04 to 182.59 ± 0.08 Ma (Burgess *et al.* 2015). A granophyric dolerite and granophyres from Tasmania yielded ages within uncertainty of the Ferrar and Dufek results (Burgess *et al.* 2015; Ivanov *et al.* 2017). Ages for three Kirkpatrick Basalt lavas also lie within uncertainty, although one is permissibly slightly younger (Burgess *et al.* 2015).

Here, the distribution and thickness of the dolerite sills are summarized, the geochemistry of the intrusive and extrusive rocks is considered, the nature of the primary basalt magma and its source in the mantle are evaluated, and the mode of emplacement of the magmas is assessed.

Distribution of dolerite sills, dykes and large intrusions

Dolerite sills are the most widespread expression of the FLIP (Gunn and Warren 1962; summarized in Elliot and Fleming 2004) and crop out in a nearly continuous belt from Horn Bluff to the Theron Mountains (Fig. 1). Sills are commonly 100–300 m thick and cumulative thicknesses of 1500 m occur where the 2.0–2.5 km-thick Devonian–Triassic Beacon sequence is most extensively developed (Barrett 1991; Collinson *et al.* 1994; Bradshaw 2013). Locally in south Victoria Land, the Basement Sill thickens to as much as 700 m (Marsh and Zeig 1997) and a 1 km-thick sill forms the 15 km-long Warren Range (Grapes and Reid 1971). The Basement Sill is estimated to have occurred continuously over an area of 10 000 km^2 in the Dry Valleys region of south Victoria Land (Marsh 2007) and appears to have a large-scale lobe structure. In north Victoria Land, intrusions present in discontinuous outcrops at identical stratigraphic positions in Beacon strata were correlated over a distance of more than 200 km (Roland and Tessensohn 1987). Sills are predominantly near parallel to bedding (Fig. 2), but none have been described that have the saucer-shape recorded, for instance, from the Karoo of South Africa (Galerne *et al.* 2008, 2011; Coetzee and Kisters 2017, 2018; Sheth 2018, fig. 8–63). A sill may merge with another sill, or may appear to be concordant with another sill with or without slivers of sedimentary rock between them. North of Mackay Glacier, south Victoria Land, massive dolerite sills are reported to coalesce and attain a thickness of more than 1000 m (Pocknall *et al.* 1994). Inclined sheets are prominent in parts of south Victoria Land (e.g. Hamilton 1965; Morrison and Reay 1995), and are reported from Mount Howe, central Transantarctic Mountains (Fig. 1) (Doumani and Minshew 1965). Massive dolerite bodies up to a few kilometres in diameter and a possible laccolith have been reported by Gunn and Warren (1962), and dyke-like bodies as much as 30 km long, 1.5–3.0 km wide and at least 1500 m in vertical outcrop by Gunn (1963). Gunn (1966) discussed a dyke-like dolerite body up to 1.6 km (1 mile) wide and inferred to extend for 24 km (15 miles) SW from just south of the Mackay Glacier; it intersects three sills, and is the feeder for the uppermost sill in that region. Gunn and Warren (1962) described dykes feeding into sills, dykes tens of metres wide and swarms of thin dykes cutting Beacon strata in south Victoria Land (e.g. Allan Hills, see Muirhead *et al.* 2012; Terra Cotta Mountain, see Morrison and Reay 1995). At Mount Gran (Fig. 3) a massive dolerite plug cuts across, and may be connected to, a number of sills of varying thickness and forming a network. The regional distribution of sills and dykes in the Dry Valleys region is documented by McElroy and Rose (1987), Woolfe *et al.* (1989), Allibone *et al.* (1991), Pocknall *et al.* (1994), Turnbull *et al.* (1994), and Isaac *et al.* (1996), and the architecture of magma emplaced into supracrustal rocks is discussed by Marsh and co-workers (Marsh 2004, 2007; see the section entitled ‘Magma emplacement at supracrustal

From: Smellie, J. L., Panter, K. S. and Geyer, A. (eds) 2021. *Volcanism in Antarctica: 200 Million Years of Subduction, Rifting and Continental Break-up*. Geological Society, London, Memoirs, **55**, 93–119,
https://doi.org/10.1144/M55-2018-39

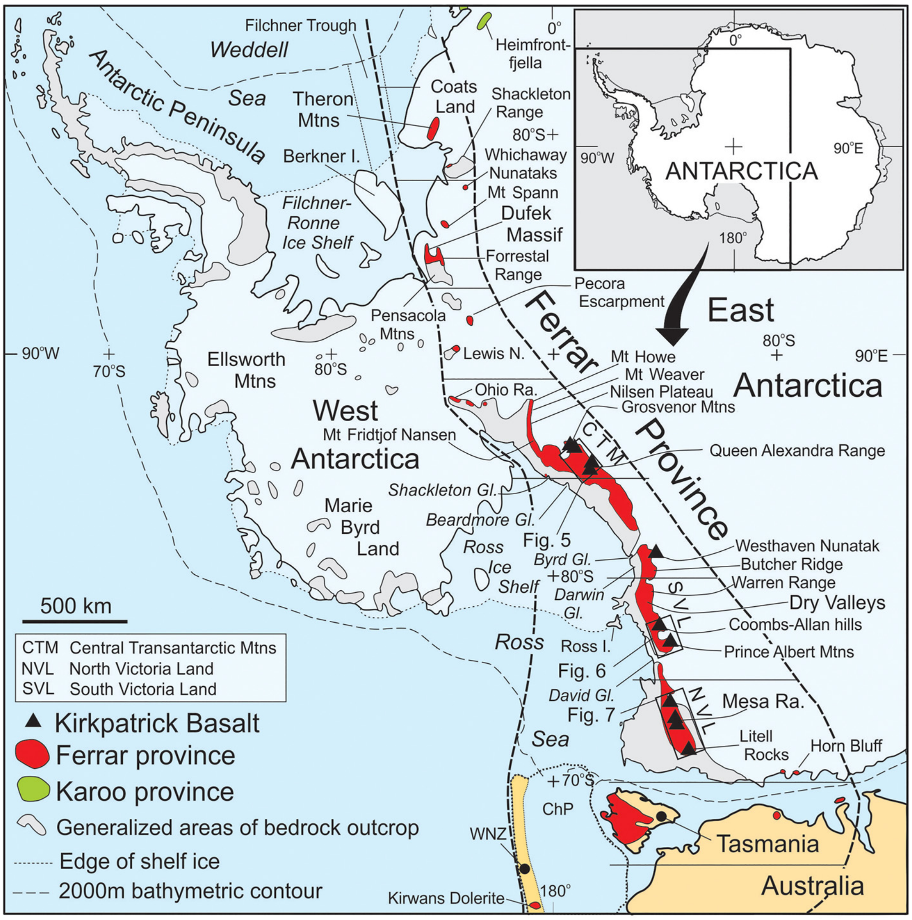

Fig. 1. Location map for the Ferrar Large Igneous Province of Antarctica and southeastern Australasia. WNZ, South Island of New Zealand west of the Alpine Fault, with the Kirwans Dolerite located. ChP, Challenger Plateau, which separates New Zealand from Australia in reconstructed Gondwana. Within the Ferrar province, the Scarab Peak Chemical Type (SPCT) has been identified in sills in the Theron Mountains and Whichaway Nunataks adjacent to the Filchner–Ronne Ice Shelf region and as the capping lava in the Transantarctic Mountains.

depths and evolution' later in this chapter). Elsewhere in the Transantarctic Mountains the numerous sills are mainly parallel to bedding, and steeply-dipping dykes are very sparsely scattered (summarized in Elliot and Fleming 2004, 2017). Dykes cutting across sills emplaced earlier are relatively rare but have been observed, mainly in the Dry Valleys region (e.g. Mount Feather, south Victoria Land, Fleming *et al.* 2005, 2012; McIntyre Promontory, central Transantarctic Mountains, Elliot and Fleming 2004). Sills may terminate in dykes, exchange stratigraphic positions, and locally form small dolerite masses and thin inclined sheets (Fig. 4). Kilometre-size dolerite masses occur locally, as in the Supporters Range and Lhasa Nunatak (Fig. 5), in the Warren Range (Fig. 1) (Grapes and Reid 1971) and Convoy Range (Fig. 6) (Pocknall *et al.* 1994), and at Butcher Ridge (Fig. 1). Aeromagnetic surveys over Butcher Ridge suggest that it is a gabbroic body about 3000 km^2 in area and with a minimum thickness of 1–2 km (Behrendt *et al.* 2002). The exposed part of the intrusion is remarkable for the inclined and contorted layers of interleaved andesite and rhyolite composition, which are cut by thin dolerite intrusions (Marshak *et al.* 1981; Shellhorn 1982; Nelson and Cottle 2016).

The layered basic Dufek intrusion (Fig. 1) (Ford and Boyd 1968; Ford 1976; Ford and Himmelberg 1991) was originally estimated, on the basis of aeromagnetic data, to have a volume of about 50 000 km^3 (Behrendt *et al.* 1981), but Ferris *et al.* (1998) argued that it comprises two much smaller bodies with a total volume of about 6600 km^3. Palaeomagnetic data have been interpreted to support the latter interpretation (Gee *et al.* 2013). More recently, Semenov *et al.* (2014) reviewed geophysical data for the Dufek intrusion, and supported the original size estimates and suggested that the smaller volume proposed by Ferris *et al.* (1998) is not consistent with petrographical observations and petrological models for layered basic intrusions.

Dolerite sills with Ferrar chemistry crop out in Tasmania (Hergt *et al.* 1989*b*) and New Zealand (Mortimer *et al.* 1995). Lavas with Ferrar chemistry are present in Tasmania (Bromfield *et al.* 2007), Kangaroo Island off South Australia (Milnes *et al.* 1982; Hergt *et al.* 1991) and in the subsurface in western Victoria (Hergt *et al.* 1991). The possibility of magma compositions similar to the Ferrar tholeiites in the Golden Gate lava sequence in the Karoo Province (Fig. 7) was suggested by Elliot and Fleming (2000), and argued for by Riley *et al.* (2006) for some of the Underberg dykes, but has yet to be confirmed. An extension of the Karoo province is present in Queen Maud Land as intrusive and extrusive rocks, and in the Theron Mountains where it forms some of the Lower Jurassic sills (Brewer *et al.* 1992; Leat 2008).

Subglacially, Ferrar tholeiites are inferred from geophysics to overlie East Antarctic basement rocks for about 500 km across the Wilkes Subglacial Basin from north Victoria Land (Ferraccioli *et al.* 2009), which is consistent with the isolated dolerite occurrences at, and to the east of, Horn Bluff. Dolerite is likewise inferred to occur for some 400 km inland from south Victoria Land (Studinger *et al.* 2004). However, Ferrar sills appear not to be present inland from the Scott Glacier toward the South Pole (Studinger *et al.* 2006). Nevertheless, it is probable that Ferrar rocks originally extended for a significant distance over the East Antarctic basement in the sector from the central Transantarctic Mountains to the Theron Mountains. Similarly, Ferrar rocks must have been present, but for a lesser distance, towards the Gondwana plate margin. Geophysical data for the Ross Ice Shelf region (Tinto *et al.* 2019) suggest that west of longitude 180° there is stretched crust related to the Lower Paleozoic Ross Orogen. If so, it is possible that Ferrar rocks extended, in the Ross embayment

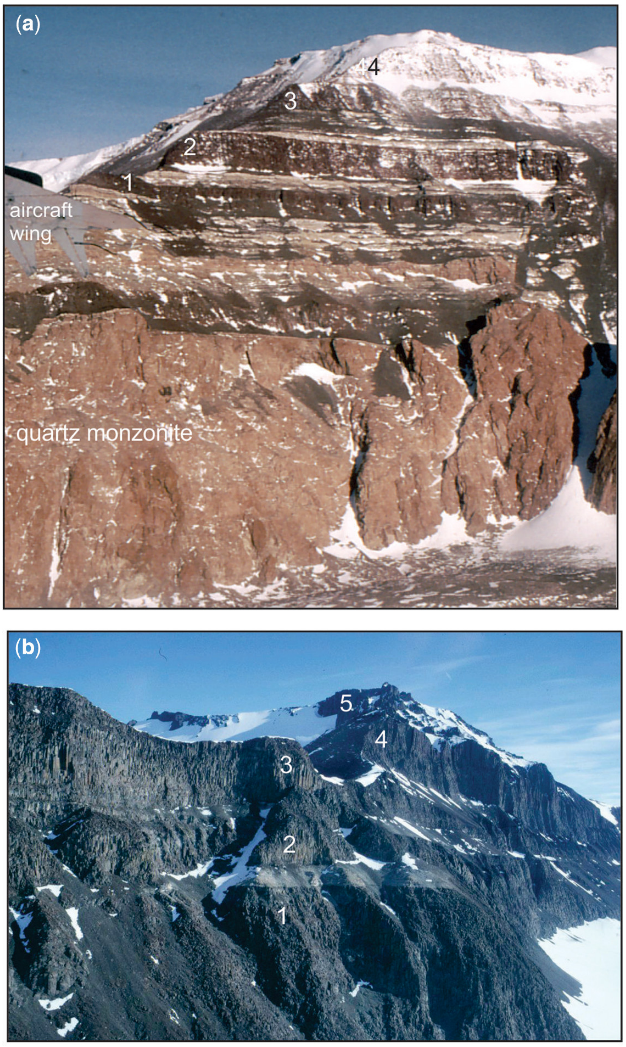

Fig. 2. (**a**) Dolerite sills at spot height 3120 m, Nilsen Plateau, central Transantarctic Mountains (Fig. 1). Sills, indicated by numbers, were intruded into Permian Beacon strata. The height of the face is about 1000 m; view to the east. (Image: D.H. Elliot.) (**b**) Stack of sills (numbered) at Mount Joyce, Prince Albert Mountains (Fig. 6). Only slivers and short stratigraphic sections of undifferentiated Beacon strata separate the sills. View to the NW; the height from the ice surface to the summit is about 800 m. Grid references for images are given in Appendix A. (Image: T.H. Fleming.)

sector, for some 200 km towards the Jurassic plate margin. Ferrar emplacement was probably limited by deformed plate margin rocks.

Prior geochemical studies

Prior (1907), in his study of the dolerites collected by the National Antarctic Expedition, 1901–04, many of which are glacial erratics from the Dry Valleys and other localities in south Victoria Land, provided the first geochemical analysis of these tholeiitic rocks. Subsequently, Benson (1916) published analyses of two tholeiite glacial erratics from Cape Royds, Ross Island, collected by the British Antarctic Expedition, 1907–09. The first analysis of an *in situ* dolerite, a rock sample from Horn Bluff that was collected by the Australasian Antarctic Expedition (1911–14), was reported by Browne (1923). The analysis of a dolerite (Stewart 1934) from Mount Fridtjof Nansen (Fig. 1) collected by L.M. Gould on the first Byrd Antarctic Expedition (1928–30) extended the

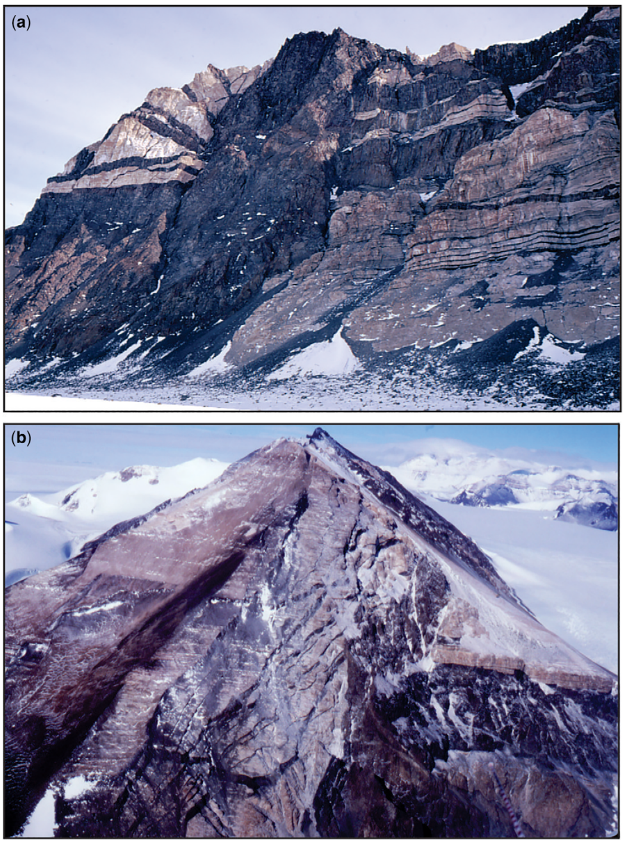

Fig. 3. (**a**) Ferrar intrusive rocks east of Mount Gran, south Victoria Land (Fig. 6). The dolerite plug cross-cuts the lowest thick sill and others higher up the rock face, and forms the feeder for other sills intruded into Devonian quartzose sandstones. View to the north; the height of the face is about 400 m. (Image: D.H. Elliot.) (**b**) Terra Cotta Mountain, south Victoria Land. Steeply inclined dolerite intrusions flank the mountain, thin dykes occur throughout the face and a climbing sill is present on the right-hand side. View to the south; the height of the face about 400 m. (Image: T.H. Fleming.)

distribution of the dolerite sills into the continental interior. Intense study of the dolerites began in the International Geophysical Year, with Gunn (1962, 1963, 1966) and Hamilton (1964, 1965) publishing the first modern investigations of sill geochemistry in south Victoria Land, and with Compston *et al.* (1968) reporting the unusually high initial Sr isotope ratio (high initial ratios of Sr had been reported previously for Tasmanian dolerites by Heier *et al.* 1965).

Subsequent studies on the chemistry of sills and lavas in south Victoria Land (the Dry Valleys region and the Prince Albert Mountains: Fig. 6), have been reported by Kyle *et al.* (1983), Morrison and Reay (1995), Wilhelm and Wörner (1996), Antonini *et al.* (1997, 1999), Demarchi *et al.* (2001), Ross *et al.* (2008) and Elliot and Fleming (2017). In particular, B.D. Marsh and collaborators (e.g. Marsh 2004, 2007; Bédard *et al.* 2007; Forsha and Zieg 2007; Zavala *et al.* 2011; Zieg and Marsh 2012) undertook a detailed investigation of the sills (Basement, Peneplain and Beacon sills) in the Dry Valleys of south Victoria Land. In north Victoria Land, north of the David Glacier (Fig. 8), the sills have been investigated by Brotzu *et al.* (1988), Hornig (1993), Antonini *et al.* (1997), Hanemann and Viereck-Götte (2004, 2007*b*), Melluso *et al.* (2014) and Elliot and Fleming (2017). Hornig (1993) reported on the sills at Scar Bluffs and Anxiety Nunataks, coastal George V Land (east of Horn Bluff). The Kirkpatrick Basalt lavas in south Victoria Land have been studied by Kyle *et al.* (1983), Wilhelm and Wörner (1996), Antonini *et al.* (1999), Demarchi *et al.* (2001) and Elliot and Fleming

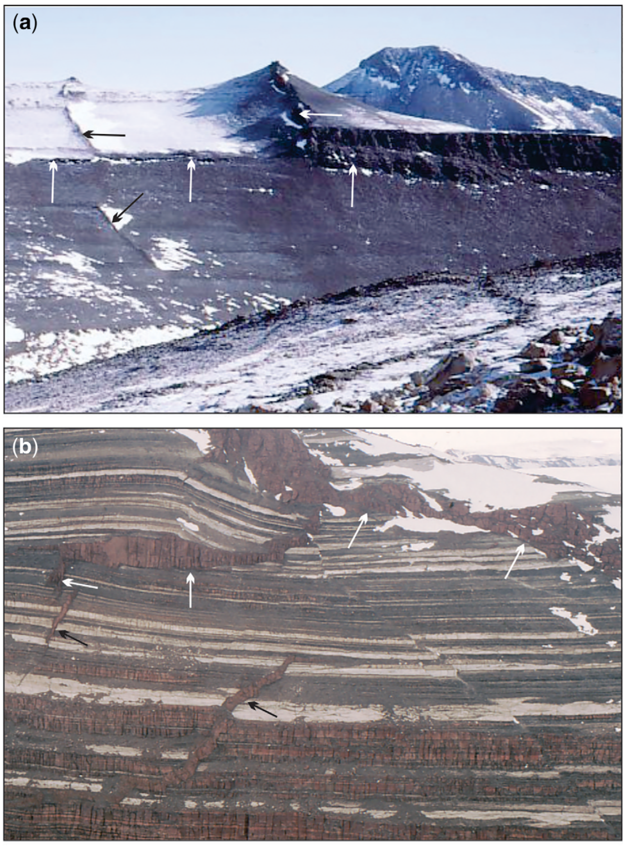

Fig. 4. (**a**) Dolerite sill (a few tens of metres thick) abruptly thinning at a dyke and continuing as a thin sill from which a second dyke extends. The head of the LaPrade Valley is immediately east of Shenk Peak (the high point in the image), view to the west, Shackleton Glacier region (Fig. 5). (Image: D.H. Elliot.) (**b**) Small dolerite dykes and masses (arrows) intruded into Triassic Fremouw Formation strata (pale sandstones and grey, slope-forming fine-grained beds); vertical bluffs of thin-bedded strata in the lower part of the image grade laterally into the slope-forming beds. View to the NE; the height of the face is about 100 m. Dismal Buttress, Shackleton Glacier region (Fig. 5). (Image: D.H. Elliot.)

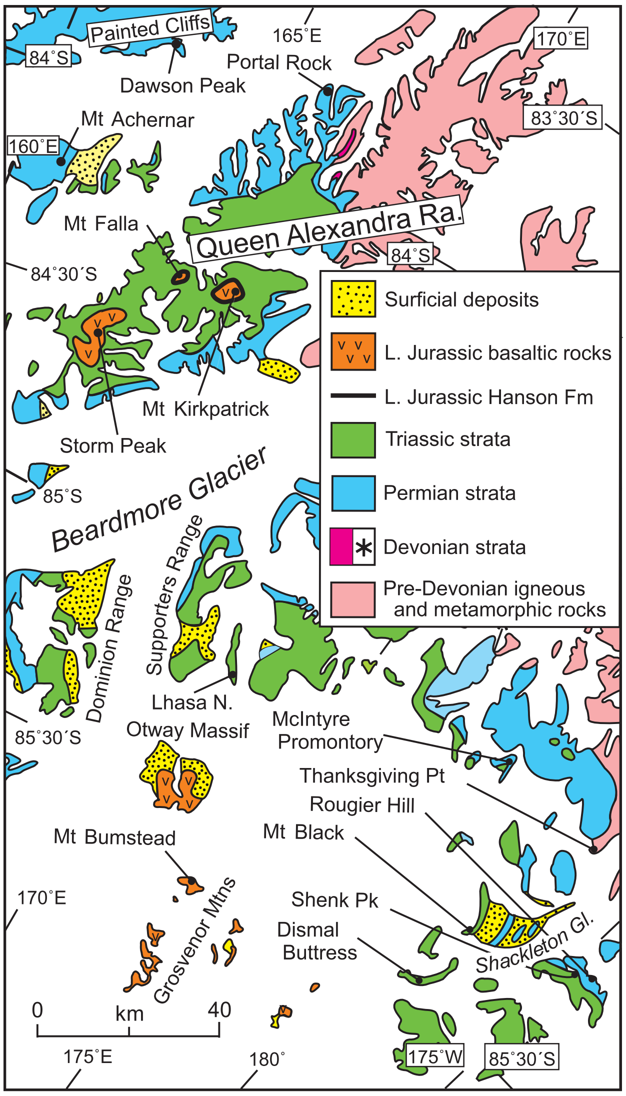

Fig. 5. Simplified geological map of the Queen Alexandra Range and Shackleton Glacier region, central Transantarctic Mountains. Ferrar Dolerite sills are co-extensive with Permian and Triassic strata. The map orientation is with north up (cf. the box in Fig. 1).

(2017). The geochemistry of the Kirkpatrick Basalt in north Victoria Land has been investigated by Mensing *et al.* (1984, 1991), Siders and Elliot (1985), Brotzu *et al.* (1988, 1992), Fleming *et al.* (1992, 1995) and Elliot *et al.* (1995). Chemical data from these studies document that the Ferrar Dolerite sills and Kirkpatrick Basalt lavas are predominantly basaltic andesite in composition. The intrusion at Butcher Ridge appears to be unique in the Ferrar province, in that it records a significant volume of silicic rocks and significant interaction with crustal rocks (Shellhorn 1982; Kyle *et al.* 1999; Nelson *et al.* 2014).

In the long stretch of the Transantarctic Mountains, from the Darwin Glacier region to the Theron Mountains (Fig. 1), the geochemistry of the lavas and sills in the central Transantarctic Mountains (Queen Alexandra Range and Shackleton Glacier region: Fig. 5) has been reported by Elliot (1970), Faure *et al.* (1974, 1991) and Elliot and Fleming (2017), for a sill at Portal Rock by Hergt *et al.* (1989*a*), and sills at Mount Achernar, central Transantarctic Mountains, and Roadend Nunatak, Darwin Glacier, by Faure *et al.* (1991). Brief information on sills at the Nilsen Plateau and the Ohio Range is given in Riley *et al.* (2020). Analyses of sills at Mount Schopf (Ohio Range), Lewis Nunatak (Thiel Mountains) and Pecora Escarpment, and dykes at Cordiner Peak (Pensacola Mountains) have been published by Ford and Kistler (1980), Vennum and Storey (1987), Leat (2008) and Harris (2014). Sills in the Theron Mountains and Whichaway Nunataks (Fig. 1) have been investigated by Stephenson (1966) and Brewer *et al.* (1992), and Ferrar dykes in the Shackleton Range reported by Stephenson (1966), Spaeth *et al.* (1995) and Leat (2008). Many of the sills in the Theron Mountains are not part of the FLIP, but geochemically are allied with the Karoo Large Igneous Province (Leat *et al.* 2006). The Dufek intrusion, a layered basic intrusion in the Pensacola Mountains (Ford and Boyd 1968, Ford and Himmelberg 1991), is part of the Ferrar province. Assuming it is a single intrusion, the lower part, the base of which is not exposed, crops out in the Dufek Massif, and the upper part, capped by a kilometre-thick granophyre, forms the Forrestal Range. A lamprophyric dyke in the Pensacola Mountains (Leat *et al.* 2000) has a similar age but is chemically very distinct and, strictly speaking, is not a Ferrar rock.

Petrography

The Dufek intrusion (Ford and Himmelberg 1991) and the thickest sills exhibit mineral layering with the associated cumulate textures. The mineralogy of the Dufek intrusion is

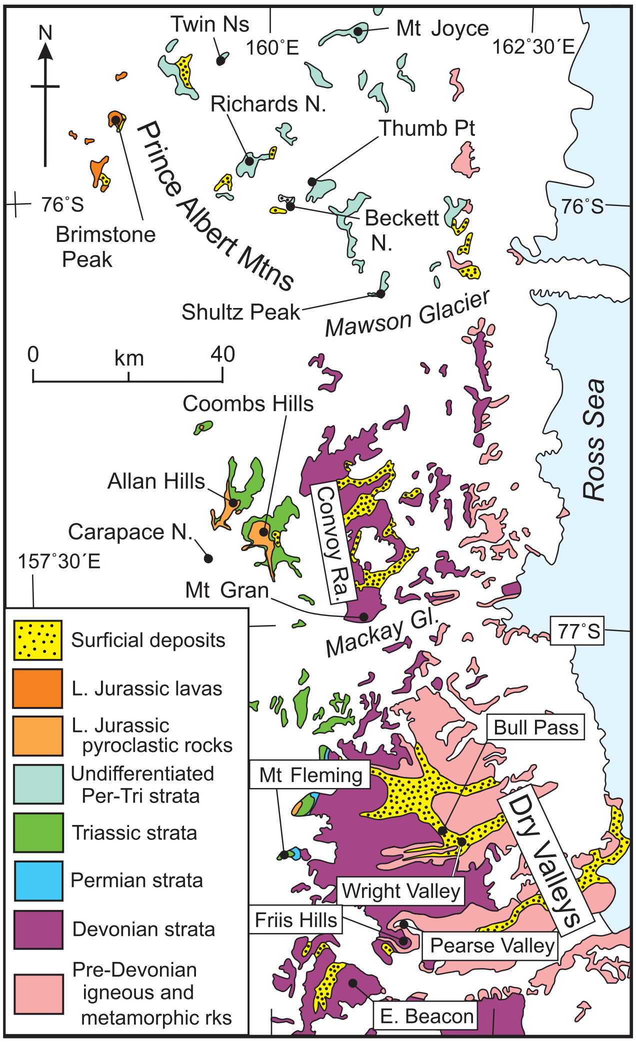

Fig. 6. Simplified geological map of south Victoria Land. Ferrar Dolerite sills are co-extensive with Devonian, Permian and Triassic strata. The map orientation is with north up (cf. the box in Fig. 1).

typical of layered basic intrusions, with plagioclase–two pyroxene (augite and pigeonite, with the latter commonly inverted to orthopyroxene) cumulates dominant, and interspersed thinner anorthosites and pyroxenites. This lower part is 1.7 km thick but the base is not exposed and might be as much as 2–3 km below the surface. This hidden basal part probably contains olivine and chromite cumulates, assuming that the Dufek is similar to other layered basic intrusions. An estimated 2–3 km-thick section is hidden beneath the snowfield between the Dufek Massif and the Forrestal Range. The upper (but not connected in outcrop) part of the intrusion (also about 1.7 km thick) in the Forrestal Range is dominated by plagioclase–two pyroxene cumulates but with more evolved compositions and significantly more iron–titanium oxides. A thick anorthosite interval occurs low in the Forrestal sequence, which is capped by a 300 m-thick granophyre.

The intensively studied Basement Sill in south Victoria Land (e.g. Bédard *et al.* 2007; Boudreau and Simon 2007; Hersum *et al.* 2007; Charrier 2010; Jerram *et al.* 2010; Zavala *et al.* 2011) includes a ponded lower zone, the Dais intrusion, in which websterite and anorthosite cumulate-textured layers up to 0.5 m thick extend continuously for several hundred metres. Although orthopyroxene and plagioclase dominate, they are accompanied by augite and inverted pigeonite, together with minor groundmass quartz, biotite and ilmenite. Layering has also been identified at Thumb Point (Fig. 6) by

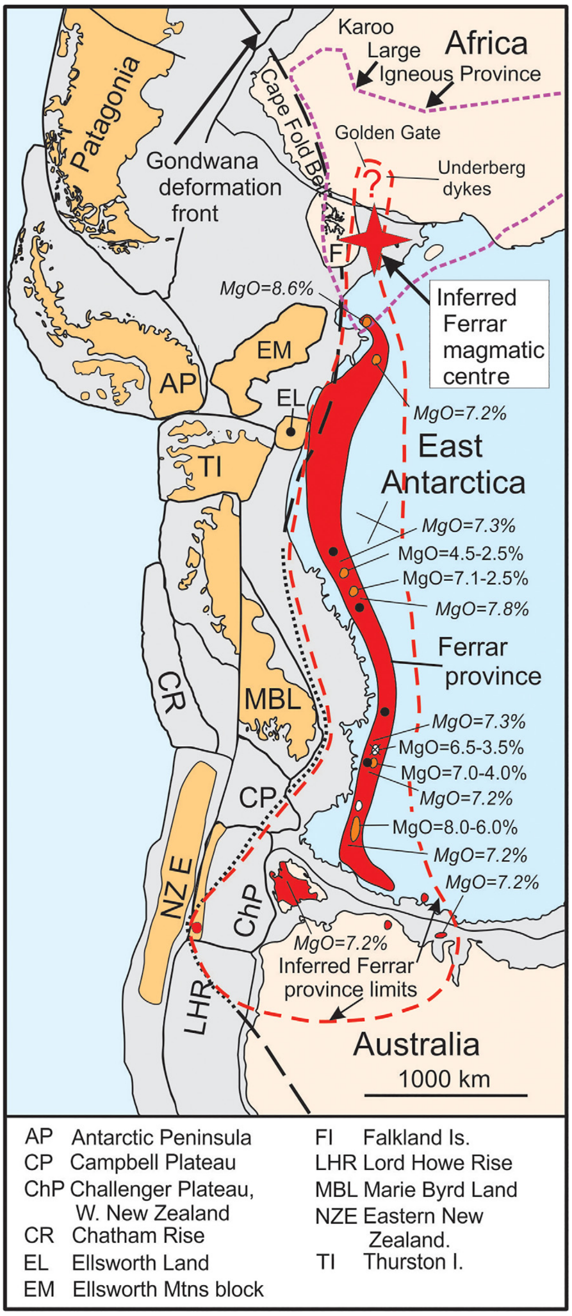

Fig. 7. Location map for the Ferrar Large Igneous Province in Gondwana (modified from a reconstruction provided by the PLATES Project at the Institute of Geophysics, University of Texas at Austin). Known outcrop areas of the SPCT composition rocks (in orange) are superimposed on the overall Ferrar distribution (SPCT compositions form sills in the Weddell Sea sector and cap the lava successions elsewhere; note there is no SPCT composition at the lava outcrop localities in white). Range of MgO compositions for lavas (excluding the SPCT composition) are linked to outcrop areas. Approximate locations of olivine-bearing dolerite sills (chilled margin MgO *c.* 9%) are marked by black dots. Sill chilled margins show no spatial pattern of compositions (highest sill MgO% in various regions is indicated in italics). The locations of possible Ferrar compositions within the Karoo Province are indicated (Golden Gate and Underberg dykes, both adjacent to Lesotho).

Ricker (1964), Gunn (1966) and Wilhelm and Wörner (1996), in several sills in the Dry Valleys by Gunn (1963), and at the Warren Range by Grapes and Reid (1971).

Chilled margins of sills may include microphenocrysts, but for the most part the sills show ophitic to doleritic textures. Excluding the Basement Sill (and possibly other unexamined

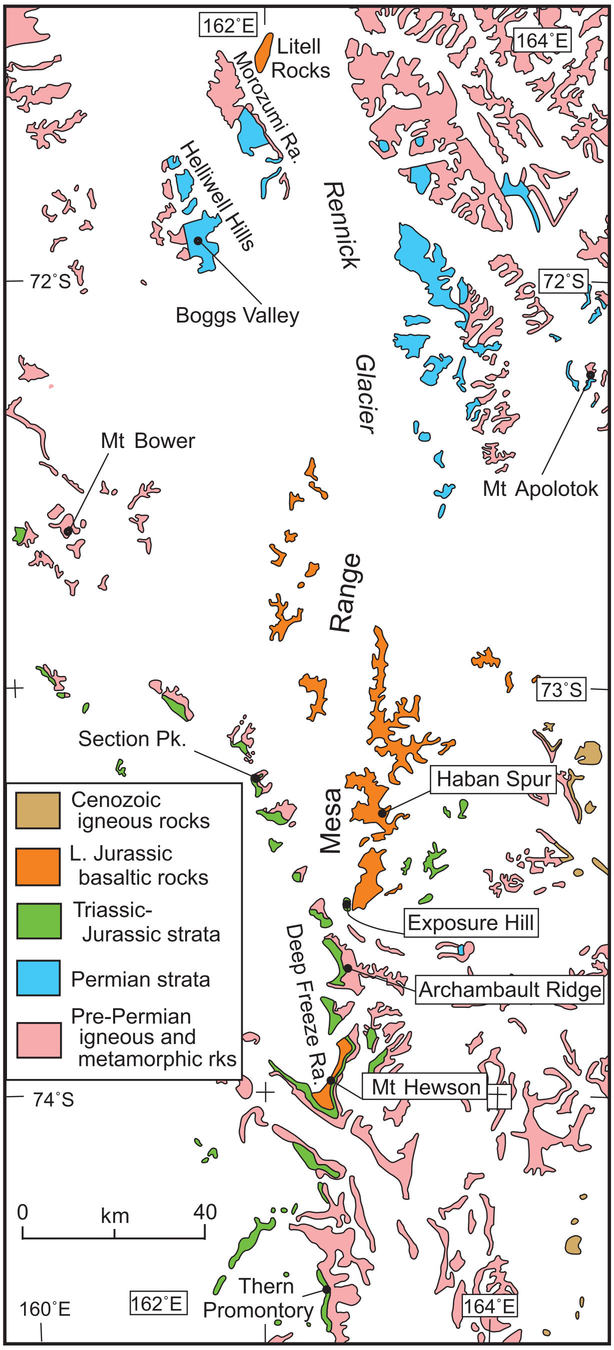

Fig. 8. Simplified geological map of north Victoria Land. Ferrar Dolerite sills are co-extensive with Permian, Triassic and Lower Jurassic (pre-Ferrar) strata. The map orientation is with north up (cf. the box in Fig. 1).

Fig. 9. Dolerite pegmatite. (**a**) A horizontal sheet. (**b**) A thin vein. Rougier Hill, Shackleton Glacier region (Fig. 5). (Images: T.H. Fleming.)

thick sills), the dolerites exhibit a narrow range of mineralogy, which is principally plagioclase (labradorite), two pyroxenes (augite and pigeonite) and iron–titanium oxides. Orthopyroxene is present in some sills with more basic compositions, and also occurs in a number of chilled margins of lava flows where it is commonly rounded; it is commonly mantled by augite. Exsolution in pyroxenes is common. Sills with the most basic composition may carry forsteritic olivine or pseudomorphs thereafter. The interstitial groundmass in the sills is mainly a quartz–feldspar intergrowth, which may be granophyric; primary biotite has been recorded in a few sills. Secondary alteration of plagioclase and mafic minerals is common. In the more differentiated sills, dolerite pegmatite (Fig. 9) or schlieren may have clinopyroxene partially replaced by amphibole, and identifiable apatite and zircon enclosed in granophyre in which sanidine has been recognized. Textures in the interior parts of thick lava flows are similar to those of the dolerite sills and the mineralogy is also similar. The mesostasis in many lavas is quite variable, and quench textures are commonly exhibited. The latter comprise feldspar microlites with needle-like overgrowths, feather-like pyroxene aggregates and skeletal iron oxides, all enclosed in lightly to strongly oxidized glass. A flow at Carapace Nunatak has a mesostasis entirely of light brown glass. Quartz–K-feldspar intergrowths range between graphic intergrowths and cryptocrystalline. A variety of accessory minerals has been recorded in the more evolved rocks at Thern Promontory, north Victoria Land (Fig. 8) (Melluso *et al.* 2014), and include fayalite, amphibole, zircon and apatite, amongst others. The granophyres in the Red Hill intrusion in Tasmania contain other trace minerals (Melluso *et al.* 2014). The sequence of liquidus phases is olivine–orthopyroxene–pigeonite–augite plus plagioclase.

The crystal size distribution has been investigated in the Basement Sill (Marsh 1998; Jerram *et al.* 2010), the Beacon (Asgard) Sill (Zieg and Marsh 2012), and in the Thumb Point sill and lavas from Brimstone Peak, south Victoria Land (Wilhelm and Wörner 1996). Wilhelm and Wörner (1996) estimated nucleation rates and cooling histories, the latter yielding estimated times of *c.* 1500 years for the sill, *c.* 200 years for the *c.* 150 m-thick capping Scarab Peak Chemical Type (SPCT) flow and <100 years for a *c.* 100 m-thick Mount Fazio Chemical Type (MFCT) flow.

Geochemistry

Many of the studies of sill geochemistry have been directed at the internal evolution, but it is the compositional range of fine-grained lavas and chilled margins of thick lavas and sills, particularly the olivine-bearing dolerite sills, that provide the context for the province-wide evolution of magmas emplaced in the uppermost crust, in supracrustal strata or at the surface. These olivine-bearing dolerite sills have MgO = *c.* 9% and constitute the least-evolved Ferrar magma compositions, and thus are regarded as the starting point for assessing both the possible magma sources in the mantle and the subsequent evolution of those primary magmas. The term olivine-bearing dolerite is used here only for those sills with chilled margins having olivine crystals and MgO = 9–10%.

As noted in the volcanology chapter (Elliot *et al.* 2021), the Ferrar magmas fall into two chemical types (Siders and Elliot 1985), designated the Mount Fazio Chemical Type (MFCT) and the Scarab Peak Chemical Type (SPCT) (Fleming *et al.* 1992). Geographically, the two chemical types overlap each other, except that the SPCT has not been recognized in SE Australasia (Fig. 7). Stratigraphically, the SPCT always forms the youngest lavas, but in the Theron Mountains occurs as a sill that is presumed to be younger than the MFCT sills. The Dufek intrusion is grouped with the MFCT lavas and sills but, without an exposed chilled margin, some uncertainty remains. The adjacent Cordiner Peaks dykes with MFCT chemistry were considered to provide the best approximation to the composition of the original Dufek magma (Ford and Kistler 1980).

The olivine-bearing dolerite composition anchors the primitive end of the MFCT trend. Both chemical types are characterized by enriched Nd and Sr initial isotope ratios, crust-like trace element patterns, and depletions in high field strength elements (HFSEs) such as Ti and P. In brief, MFCT rocks (excluding the Dufek intrusion) have a range of compositions ($^{87}Sr/^{86}Sr_i$ = *c.* 0.7081–0.7138; MgO = 9.2–2.6%; Zr = 60–175 ppm), whereas the SPCT has a restricted composition ($^{87}Sr/^{86}Sr_i$ = *c.* 0.7095; MgO = *c.* 2.3%; Zr = *c.* 230 ppm). Comparisons between the two are discussed later. Although the timing of the Ferrar and Karoo provinces is nearly identical (Svensen *et al.* 2012; Sell *et al.* 2014), the geochemistry is quite distinct. Karoo basic magmas are much more diverse and, with a few exceptions, are geochemically distinct, having, for example, less enriched Sr, Nd and Pb isotopic compositions, and higher HFSE concentrations (Marsh *et al.* 1997; Jourdan *et al.* 2007; Neumann *et al.* 2011; Heinonen *et al.* 2014).

Previous studies of the Ferrar tholeiites have been cited in the introduction to this section. Those investigations acquired data in various analytical laboratories, and therefore comparisons between datasets are hampered by differences in precision and accuracy, by inter-laboratory biases, and, in the case of isotope measurements, by different and evolving standards and precisions. This concern is illustrated by the analysis of 10 SPCT samples distributed between the Mesa Range and the Grosvenor Mountains, which showed that the variations in concentrations, excluding the more mobile elements, fall within analytical precisions (Elliot *et al.* 1999; see also Fleming *et al.* 1992). Other authors (Hornig 1993; Molzahn *et al.* 1996; Antonini *et al.* 1997) have analysed SPCT samples, but results differ markedly for some elements, although are similar for others. Presentation of all the existing data leads to considerable analytical scatter and expanded fields, which, although broadly showing trends, lacks the clarity needed for an accurate portrayal of petrogenetic relationships. Further, alteration affects at least the more mobile elements, thus producing a ‘geological’ scatter of data, let alone the high-temperature hydrothermal exchange affecting Sr isotope compositions that may occur in chilled margins of sills. Finally, it is not always evident exactly where an analysed sample was collected in either a lava or a sill, and thus the possible effects of *in situ* differentiation are often unclear. The data presented here have been selected in an attempt to reduce these biases and uncertainties, and therefore have been drawn from the authors’ studies of the Ferrar rocks extending geographically from the Mesa Range to the Nilsen Plateau (Fig. 1). Data are presented for samples that span the full range of magma compositions. In most cases this is illustrated using previously unpublished Ferrar mineral and whole-rock data from the central Transantarctic Mountains. Data sources are given in the figure captions.

Mineral chemistry

Early studies (e.g. Gunn 1966) reported mineral compositions determined by optical methods. Here, only mineral compositions determined by electron microprobe are considered. The Dufek intrusion is discussed separately.

Feldspar. MFCT plagioclase compositions typically range from calcic bytownite to calcic andesine, whereas the SPCT plagioclase has a more restricted range from calcic labradorite to sodic andesine (Table 1; Fig. 10) (Brotzu *et al.* 1992; Fleming 1995; Elliot *et al.* 1995; Antonini *et al.* 1999; Demarchi *et al.* 2001; Hanemann and Viereck-Götte 2004; Melluso *et al.* 2014). The more sodic plagioclase occurs as rims and groundmass grains. The groundmass may include alkali feldspar, which ranges from albite to orthoclase and even sanidine, with the K-feldspars occurring in granophyric intergrowths and granophyres (Barrett *et al.* 1986; Hornig 1993; Melluso *et al.* 2014). Anorthoclase has also been reported by the latter two authors. Plagioclase in the Dais layered body in the Basement Sill, south Victoria Land (Bédard *et al.* 2007) occurs in a variety of distinct textural settings (e.g. cumulate crystals, inclusions in other minerals, schlieren). The overwhelming composition is sodic bytownite in the chilled margin and lower gabbronorite, and calcic bytownite in the overlying rocks, but with some more sodic rim compositions; oligoclase is present in pegmatitic schlieren.

Pyroxene. Excluding the Basement Sill in the Dry Valleys and other sills with cumulates, orthopyroxene is present in a number of MFCT lavas and sills, and also occurs in chilled margins (Brotzu *et al.* 1992; Hornig 1993; Elliot *et al.* 1995; Fleming 1995; Antonini *et al.* 1999; Demarchi *et al.* 2001; Hanemann and Viereck-Götte 2004; Melluso *et al.* 2014). The most Mg-rich pigeonite (Mg# *c.* 84: Mg# = (Mg/[Mg + Fe] × 100) may co-exist with orthopyroxene (Mg# *c.* 85), and those and many other pyroxenes may exhibit marked Fe-enrichment both in rims and as core compositions in the more evolved tholeiites (Fig. 10). Augite similarly shows Fe-enrichment in grain rims (Mg# *c.* 20). The pyroxenes in lavas include compositions that bridge the gap between augite and pigeonite, which reflects quenching. Hedenbergitic pyroxenes (with Mg# <10) are present in the most-evolved MFCT compositions (Melluso *et al.* 2014). The SPCT pyroxene compositions (only pigeonite and augite) are relatively restricted (Table 2; Fig. 10), and also exhibit Fe-enriched rims. Based on the two-pyroxene geothermometer (Ishii 1975; Lindsley 1983; Lindsley and Andersen 1983), temperatures of crystallization for MFCT rocks range from 1200 to 1050°C for the lavas, and as low as 850°C for the more evolved rocks, and for SPCT lavas 1105–1070°C (Brotzu *et al.* 1992; Elliot *et al.* 1995; Fleming 1995; Melluso *et al.* 2014).

In the Dais intrusion (the basal part of the Basement Sill) the majority of primocryst orthopyroxenes have Mg# >80, with a scattering down to Mg# *c.* 65 (Bédard *et al.* 2007). Ca-rich clinopyroxenes in the lower part of the intrusion have Mg# >70

Table 1. *Plagioclase compositions determined by microprobe analysis for samples from Dawson Peak and Storm Peak*

Sample Type Region	85-71-1 MFCT Sill CTM	85-71-1 MFCT Sill CTM	85-75-1 MFCT Lava CTM	85-75-9 MFCT Lava CTM	85-75-13 MFCT Lava CTM	85-76-39 MFCT Lava CTM	85-76-39 MFCT Lava CTM	85-76-54 MFCT Lava CTM	85-76-54 MFCT Lava CTM	85-76-60 SPCT Lava CTM	85-76-60 SPCT Lava CTM
SiO_2	45.87	50.09	48.69	51.24	50.08	48.79	52.38	50.52	53.64	53.37	55.49
Al_2O_3	33.77	31.12	32.11	30.36	30.98	32.16	28.92	31.04	28.27	29.04	27.43
FeO	0.45	0.76	0.48	0.83	0.88	0.58	0.8	1.06	1.08	1.02	0.72
MgO	0.15	0.40	0.29	0.17	0.09	0.21	0.13	0.05	0.07	0.01	0.05
CaO	17.60	13.71	15.55	13.94	13.94	16.17	12.44	14.18	11.49	11.83	9.65
Na_2O	1.24	3.03	2.44	3.21	3.08	2.16	4.09	3.01	4.54	4.57	5.33
K_2O	0.07	0.23	0.12	0.19	0.21	0.10	0.31	0.19	0.37	0.22	0.45
Total	99.14	99.33	99.67	99.94	99.27	100.17	99.07	100.06	99.48	100.07	99.11
Si^{4+}	2.132	2.300	2.238	2.339	2.304	2.234	2.405	2.310	2.449	2.423	2.523
Al^{3+}	1.850	1.684	1.739	1.633	1.680	1.736	1.565	1.672	1.512	1.554	1.470
Fe^{2+}	0.018	0.029	0.019	0.032	0.034	0.022	0.031	0.041	0.041	0.039	0.027
Mg^{2+}	0.010	0.027	0.020	0.011	0.006	0.014	0.009	0.003	0.005	0.001	0.004
Ca^{2+}	0.876	0.675	0.765	0.682	0.687	0.793	0.612	0.695	0.562	0.576	0.470
Na^{+}	0.111	0.270	0.217	0.284	0.275	0.191	0.364	0.267	0.402	0.403	0.470
K^{+}	0.004	0.013	0.007	0.011	0.013	0.006	0.018	0.011	0.022	0.013	0.026
Total	5.001	4.999	5.005	4.992	4.999	4.997	5.004	4.995	4.993	5.008	4.990
O^{2-}	8.000	8.000	8.000	8.000	8.000	8.000	8.000	8.000	8.000	8.000	8.000
An	88.4	70.5	77.3	69.8	70.5	80.1	61.6	71.4	57.0	58.1	48.7
Ab	11.2	28.2	21.9	29.1	28.2	19.3	36.6	27.5	40.8	40.6	48.6
Or	0.4	1.4	0.7	1.1	1.3	0.6	1.8	1.1	2.2	1.3	2.7

Analyses were performed at the Ohio State University Electron Microprobe Laboratory.
The analyses have been selected to show the range of compositions represented by the olivine-bearing dolerite sill at Dawson Peak and the lavas at Storm Peak. Analysis 85-75-1 is for the basal, thin basic flow. Samples 85-75-9 and 85-75-13 are from the 135 m-thick tachylitic flow 2. The two analyses for samples 85-76-39 (flow 13), 85-76-54 (flow 14) and 85-76-60 (flow 15) represent the range of compositions in those flows. Sample 85-76-60 is the SPCT flow. Data are from Fleming (1995).

with less Mg-rich augites more common in the upper part (Bédard *et al.* 2007).

Olivine. Olivine, or pseudomorphs after olivine, occurs principally in sills and has been recorded in south Victoria Land (Thumb Point, Gunn 1966; Skinner and Ricker 1968; Wilhelm and Wörner 1996: Roadend Nunatak, Hergt *et al.* 1989*a*), in the Queen Alexandra Range region (Painted Cliffs, Gunn 1966; Dawson Peak, Fleming 1995) and at Nilsen Plateau (McLelland 1967). In the olivine-bearing dolerite sills the composition range is Fo_{77}–Fo_{88} (Table 2; Fig. 10) (see Fleming 1995). Pseudomorphs after olivine have been noted only in one flow from north Victoria Land (Fleming *et al.* 1995). Melluso *et al.* (2014) reported fayalitic olivine as a rare groundmass phase in evolved rocks from Thern Promontory, north Victoria Land, and from granophyre at Red Hill, Tasmania (Fo_2–Fo_6).

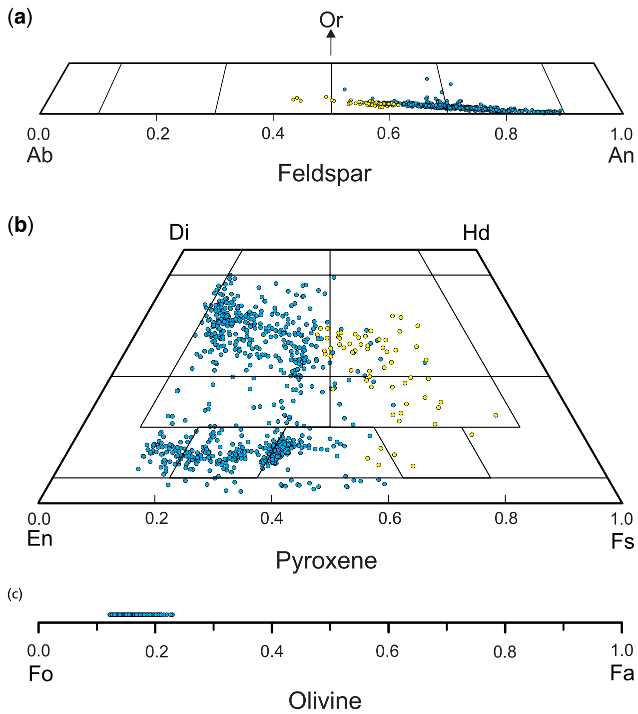

Fig. 10. Compositional variation preserved in minerals from sills at Dawson Peak and lavas at Storm Peak determined by electron microprobe analysis. (**a**) Plagioclase. (**b**) Pyroxene. (**c**) Olivine. Plagioclase from MFCT samples are in blue, SPCT samples are in yellow. Data source: Fleming (1995).

Oxides. Titanomagnetite with exsolved ilmenite is a common accessory mineral in the lavas and sills (Brotzu *et al.* 1992; Hornig 1993; Elliot *et al.* 1995; Fleming 1995). Temperature of subsolidus re-equilibration was estimated to be *c.* 870°C. Titanomagnetite grains lacking exsolution lamellae lie in the range $Usp_{56–76}$. Independent ilmenite occurs in sills. Melluso *et al.* (2014) reported co-existing magnetite and ilmenite in evolved rocks, and calculated temperatures of crystallization of *c.* 750–820°C. Chromite occurs as inclusions in olivine and as independent grains in an olivine-bearing dolerite sill analysed by Fleming (1995), who reported that the independent grains are zoned (Cr# = 48–69: $Cr\# = (Cr^3/[Cr^3 + Al^3] \times 100)$) and rimmed by titanomagnetite.

Dufek intrusion. Plagioclase cores in the Dufek intrusion have a limited compositional range (An_{50}–An_{79}) but individual grains exhibit little zoning (Ford and Himmelberg 1991), most probably due to annealing. The lower part of the intrusion is unexposed; however, orthopyroxene, with Mg# *c.* 70, present in the lowest exposed rock unit is replaced by pigeonite low in the section and is present up into the upper gabbros, becoming more Fe-rich (Mg# *c.* 40) (Himmelberg and Ford 1976). Ca-rich pyroxene is increasingly Fe-rich throughout

Table 2. *Pyroxene and olivine compositions determined by microprobe analysis for Ferrar rocks from Dawson Peak and Storm Peak*

Sample	**85-71-1**	**85-71-1**	**85-75-1**	**85-75-1**	**85-75-9**	**85-75-9**	**85-75-9**	**85-75-36**	**85-76-36**	**85-76-63**	**85-76-63**	**85-71-2**	**85-71-2**
Type	**MFCT**	**MFCT**	**MFCT**	**MFCT**	**MFCT**	**MFCT**	**MFCT**	**MFCT**	**MFCT**	**SPCT**	**SPCT**	**MFCT**	**MFCT**
	Sill	**Sill**	**Lava**	**Lava**	**Lava**	**Lava**	**Lava**	**Lava**	**Lava**	**Lava**	**Lava**	**Sill**	**Sill**
	pig	**aug**	**pig**	**aug**	**pig**	**subcalcic**	**aug**	**pig**	**aug**	**pig**	**aug**	**ol**	**ol**
Region	**CTM**	**CTM**	**CTM**	**CTM**	**CTM**	**CTM**	**CTM**	**CTM**	**CTM**	**CTM**	**CTM**	**CTM**	**CTM**
SiO_2	55.09	52.84	52.06	52.93	51.59	50.35	48.42	52.18	52.71	49.12	49.17	39.81	38.28
TiO_2	0.15	0.27	0.20	0.21	0.29	0.73	1.14	0.40	0.24	0.43	0.74		
Al_2O_3	2.40	2.79	0.68	1.18	0.93	1.91	3.26	1.38	0.78	0.82	1.48	0.03	0.03
FeO	8.58	7.14	20.32	8.51	22.51	19.87	17.83	11.57	17.96	30.79	20.58	13.05	20.89
MnO	0.25	0.17	0.41	0.32	0.48	0.43	0.38	0.19	0.46	0.62	0.45	0.24	0.32
MgO	27.94	18.48	20.25	18.62	18.6	15.08	12.60	16.06	22.31	12.99	10.55	46.10	39.44
CaO	4.66	17.75	4.97	17.36	4.98	10.51	15.06	17.85	4.47	4.07	15.51	0.21	0.09
Na_2O	0.04	0.11	0.08	0.08	0.03	0.14	0.14	0.15	0.05	0.02	0.07		
Cr_2O_3	1.07	0.24	0.02	0.06	0.04	0.01	0.11	0.11	0.05	0.00	0.02		
NiO												0.27	0.10
Total	100.17	99.79	98.99	99.27	99.45	99.03	98.95	99.88	99.02	98.86	98.57	99.71	99.14
Si^{4+}	1.945	1.932	1.971	1.958	1.964	1.936	1.877	1.950	1.968	1.960	1.940	0.996	0.999
Ti^{4+}	0.004	0.007	0.006	0.006	0.008	0.021	0.033	0.011	0.007	0.013	0.022		
Al^{3+}	0.100	0.120	0.030	0.052	0.042	0.087	0.149	0.061	0.034	0.039	0.069	0.001	0.001
Fe^{2+}	0.253	0.218	0.644	0.263	0.717	0.639	0.579	0.361	0.561	1.028	0.679	0.273	0.456
Mn^{2+}	0.007	0.005	0.013	0.010	0.016	0.014	0.013	0.006	0.014	0.021	0.015	0.005	0.007
Mg^{2+}	1.470	1.007	1.143	1.027	1.055	0.865	0.729	0.895	1.242	0.773	0.621	1.718	1.534
Ca^{2+}	0.176	0.695	0.197	0.688	0.203	0.433	0.625	0.715	0.179	0.174	0.656	0.006	0.003
Na^{+}	0.003	0.008	0.006	0.006	0.002	0.010	0.011	0.011	0.003	0.002	0.005		
Cr^{3+}	0.030	0.007	0.001	0.002	0.001	0.000	0.010	0.003	0.001	0.000	0.001		
NiO												0.005	0.002
Total	3.988	4.001	4.011	4.012	4.008	4.004	4.021	4.013	4.009	4.009	4.006	3.004	3.001
O^{2-}	6.000	6.000	6.000	6.000	6.000	6.000	6.000	6.000	6.000	6.000	6.000	4.000	4.000
Wo	9.3	36.2	10.1	34.8	10.3	22.4	32.4	36.3	9.0	8.8	33.5		
En	77.4	52.4	57.5	51.9	53.4	44.6	37.7	45.4	62.7	39.1	31.7		
Fs	13.3	11.4	32.4	13.3	36.3	33.0	29.9	18.3	28.3	52.0	34.7		
Fo												86.3	77.1
Fa												13.7	22.9

Analyses performed at the Ohio State University Electron Microprobe Laboratory.

The analyses represent the range of pyroxene and olivine compositions in the olivine-bearing dolerite sill at Dawson Peak and in the lavas at Storm Peak, central Transantarctic Mountains. Pyroxene compositions: olivine-bearing dolerite 85-71-1; analysis 85-75-1 is for the basal, thin basic flow; sample 85-75-9 is from the 135 m-thick tachylitic flow 2; the two analyses for samples 85-76-36 (flow 12) and 85-76-63 (flow 15) represent the range in compositions in those flows; sample 85-76-63 is the SPCT flow. Olivine compositions are from olivine-bearing dolerite sill sample 85-71-2. Data are from Fleming (1995).

the intrusion, ranging between Mg# *c.* 75 and Mg# *c.* 35. Temperatures of crystallization were estimated to be in the range 1180–1040°C, falling to about 800°C for the late stages. Forsteritic olivine does not occur in the lower part of the intrusion, indicating that a thick section is most likely to be concealed beneath the surface. The rare occurrence of fayalitic olivine in the upper part of the intrusion has been noted (Himmelberg and Ford 1976). The common oxide is titanomagnetite with ilmenite exsolution lamellae; independent ilmenite is rare (Himmelberg and Ford 1977). Preliminary results of ongoing investigations were reported in Grimes *et al.* (2008) and Carnes *et al.* (2011).

Major and trace element geochemistry

The Ferrar tholeiites (Ford and Kistler 1980; Kyle 1980; Mensing *et al.* 1984, 1991; Siders and Elliot 1985; Brotzu *et al.* 1988, 1992; Faure *et al.* 1991; Brewer *et al.* 1992; Fleming *et al.* 1992, 1995; Hornig 1993; Elliot *et al.* 1995; Fleming 1995; Morrison and Reay 1995; Wilhelm and Wörner 1996; Antonini *et al.* 1997, 1999; Demarchi *et al.* 2001; Hanemann and Viereck-Götte 2004, 2007*b*; Ross *et al.* 2008; Melluso *et al.* 2014; Elliot and Fleming 2017) constitute two distinct compositional groups: the bulk of the rocks belong to the Mount Fazio Chemical Type (MFCT) and the remaining *c.* 1% to the Scarab Peak Chemical Type (SPCT) (Fleming *et al.* 1992). Representative chemical analyses are presented in Table 3; in the Province overall, the SPCT has a markedly restricted composition (Mg# = 22–24), whereas the MFCT has a broad range of compositions (Mg# *c.* 11–69), with the olivine-bearing dolerite sill margins representing the most primitive liquid compositions and having the highest Mg numbers. Evolved tholeiite samples from Thern Promontory have the lowest Mg numbers. There is some uncertainty as to whether these Thern Promontory rocks represent a lava sequence or just two sills (see Brotzu *et al.* 1988, 1992: Lanza and Zanella 1993; Melluso *et al.* 2014; the authors, who have not visited the locality, prefer the sill interpretation, in which case the highly evolved compositions, with MgO concentrations as low as 0.6%, reflect *in situ* differentiation within a sill interior, a view supported by L. Viereck pers. comm. June 2018). The bulk of the lavas have MgO between 2.5 and 7.5%. High MgO (>7.5%) in some thicker lavas represents an accumulation of pyroxene and reflects *in situ* differentiation in those flows, which is supported by relatively high Cr and Ni. Coherent trends on variation diagrams for fine-grained rocks (Fig. 11) demonstrate the MFCT forms a related set of magma compositions. Large ion lithophile elements (LILEs) show marked scatter, which is greatly reduced if those analyses with high loss-on-ignition are excluded (e.g. Fleming *et al.* 1992). HFSEs show regular increases with decreasing Mg number. Incompatible elements plotted on a mid-ocean ridge basalt (MORB)-normalized diagram

Table 3. *Major and trace element analyses of a sill (85-72-2) at Dawson Peak, nine MFCT lavas and one SPCT lava at Storm Peak*

Sample Type	85-72-2 Sill	85-75-1 Flow 1	85-76-39 Flow 13	85-76-36 Flow 12	85-76-33 Flow 11	85-76-20 Flow 8	85-76-17 Flow 7	85-76-29 Flow 10	85-76-23 Flow 9	85-76-49 Flow 14	85-75-11 Flow 2	85-76-60 Flow 15
SiO_2	52.68	54.26	55.46	57.25	57.99	59.10	57.89	58.90	59.41	58.66	59.71	57.85
TiO_2	0.49	0.66	0.95	1.25	1.37	1.43	1.55	1.53	1.56	1.62	1.52	2.00
Al_2O_3	16.22	15.49	14.26	13.58	13.34	13.14	12.99	12.79	12.91	12.87	12.56	12.07
Fe_2O_3	1.06	1.14	1.38	1.45	1.49	1.50	1.60	1.55	1.52	1.60	1.57	1.84
FeO	7.04	7.57	9.17	9.63	9.94	10.02	10.64	10.32	10.16	10.67	10.45	12.25
MnO	0.16	0.20	0.19	0.18	0.18	0.19	0.22	0.18	0.18	0.18	0.18	0.19
MgO	9.15	7.08	5.71	4.44	3.81	3.28	3.34	3.21	2.90	2.93	2.61	2.28
CaO	11.36	9.59	9.07	8.80	8.38	8.07	7.32	7.48	7.56	7.65	7.23	7.05
Na_2O	1.54	3.36	2.33	2.19	2.47	2.42	1.94	2.05	2.39	2.71	2.26	2.39
K_2O	0.23	0.58	1.36	1.07	0.86	0.68	2.34	1.81	1.24	0.92	1.72	1.83
P_2O_5	0.06	0.10	0.13	0.15	0.17	0.17	0.19	0.17	0.18	0.20	0.19	0.26
Total	100.00	100.00	100.00	100.00	100.00	100.00	100.00	100.00	100.00	100.00	100.00	100.00
LOI	1.13	1.89	1.46	0.83	0.97	1.03	3.15	1.84	0.82	1.55	0.90	0.36
Mg#	69.8	62.5	52.6	45.1	40.6	36.9	35.9	35.7	33.7	32.9	30.8	24.9
Trace elements by XRF (Ni, Cr, Sr, Zr) and ICP-MS												
Ni	119	66	49	32	23	13	13	13	11	12	6	8
Cr	398	109	47	43	32	28	25	27	24	17	18	15
Rb	6.9	11.7	42.2	59.0	65.6	73.2	53.0	65.0	68.5	78.1	75.6	67.1
Sr	111	101	132	135	134	137	66	136	141	131	136	124
Y	15.9	22.0	28.8	36.4	37.1	40.2	37.1	38.6	41.1	43.3	39.5	53.6
Zr	58	94	121	151	162	172	180	172	177	184	180	202
Nb	2.84	5.26	6.78	9.78	9.84	10.57	10.14	10.80	11.59	10.62	10.82	10.79
Cs	0.52	0.74	1.01	2.09	2.50	4.03	1.47	2.57	2.91	3.19	2.79	1.56
Ba	70	377	264	296	292	315	414	355	366	335	380	383
La	6.64	11.66	15.70	20.80	22.75	23.55	22.74	23.76	24.97	26.21	25.18	26.09
Ce	13.11	23.89	31.44	41.88	45.00	48.11	45.63	47.81	50.05	52.37	50.49	54.14
Pr	1.60	2.88	3.69	4.98	5.35	5.66	5.40	5.54	5.89	6.16	5.85	6.48
Nd	6.76	12.02	15.29	20.20	21.41	23.52	22.27	22.81	24.71	25.37	24.16	26.98
Sm	1.95	3.08	4.09	5.12	5.54	5.84	5.85	5.86	6.09	6.51	6.22	7.53
Eu	0.64	0.92	1.04	1.28	1.39	1.42	1.37	1.40	1.55	1.52	1.52	1.84
Gd	2.13	3.23	4.26	5.29	5.60	6.05	5.72	5.64	5.97	6.23	6.03	7.92
Tb	0.41	0.63	0.81	0.97	1.01	1.12	1.03	1.04	1.13	1.22	1.09	1.51
Dy	2.69	4.08	5.22	6.05	6.50	6.89	6.81	6.62	6.96	7.50	6.94	9.80
Ho	0.62	0.83	1.12	1.28	1.39	1.47	1.43	1.38	1.50	1.58	1.49	2.05
Er	1.79	2.49	3.35	3.78	3.98	4.24	4.19	4.06	4.26	4.78	4.49	6.10
Tm	0.25	0.36	0.47	0.55	0.57	0.61	0.58	0.58	0.62	0.68	0.63	0.85
Yb	1.60	2.27	2.85	3.45	3.49	3.82	3.69	3.68	3.83	4.12	3.98	5.41
Lu	0.26	0.36	0.48	0.52	0.57	0.61	0.61	0.59	0.62	0.65	0.61	0.83
Hf	1.40	2.37	3.19	3.89	4.38	4.58	4.64	4.66	4.87	5.01	4.93	5.70
Ta	0.22	0.34	0.46	0.58	0.65	0.68	0.70	0.69	0.72	0.75	0.74	0.86
Pb	2.86	5.69	7.33	9.16	10.31	17.14	11.60	10.98	11.83	11.62	12.08	11.68
Th	1.47	2.77	3.86	4.98	5.61	5.91	6.02	6.01	6.26	6.51	6.49	6.31
U	0.29	0.58	0.83	1.02	1.16	1.29	1.22	1.25	1.28	1.34	1.35	1.23

LOI, loss on ignition.
Analyses recalculated to 100%.
Iron partitioned: $Fe_2O_3/FeO = 0.15$.
Analyses were performed at the GeoAnalytical Laboratory at Washington State University.

(Fig. 12) highlight the crust-like patterns of the Ferrar rocks. Rare earth element (REE) diagrams (Fig. 13) illustrate patterns typical of continental tholeiites: enriched light REE but flat patterns for medium REE and heavy REE, with a negative Eu anomaly except in the olivine-bearing dolerite compositions, indicate the role of plagioclase during differentiation at crustal depths. Platinum group elements (PGEs) in north Victoria Land tholeiites (Hanemann and Viereck-Götte 2007*a*) show modest correlations with MgO (or Mg#). A detailed investigation of the PGEs in the Basement Sill in south Victoria Land revealed a positive correlation between Os and Ir at MgO less than 8%, and positive (convex-shaped) slopes between the Os–Ir–Ru group and the Pt–Pd–Rh group (Choi *et al.* 2019*a*). Preliminary results of investigations into PGEs in the Dufek intrusion have been reported by Mukasa *et al.* (2007) and Hanemann *et al.* (2009).

On a classical AFM diagram (Fig. 14), the MFCT compositions exhibit strong Fe-enrichment typical of tholeiitic rocks, with the Thern Promontory rocks (Melluso *et al.* 2014) and an interstitial glass from a Mesa Range lava (Elliot *et al.* 1995) showing the most extreme *in situ* tholeiitic magma evolution (although none is likely to be a liquidus composition). The extreme Fe-enrichment (Fe^t *c.* 14%) of the SPCT rocks is comparable to that of ferrobasalts from mid-ocean ridges.

Olivine-bearing dolerite sills are known to crop out in the central Transantarctic Mountains and south Victoria Land but not north Victoria Land; however, this may simply be an artefact of exposure or lack of discovery. The lavas, however, show regional variations in predominant major element compositions (Elliot and Fleming 2017). The majority of lavas in the central Transantarctic Mountains are evolved with only a few having Mg# >45, whereas in south Victoria Land lavas

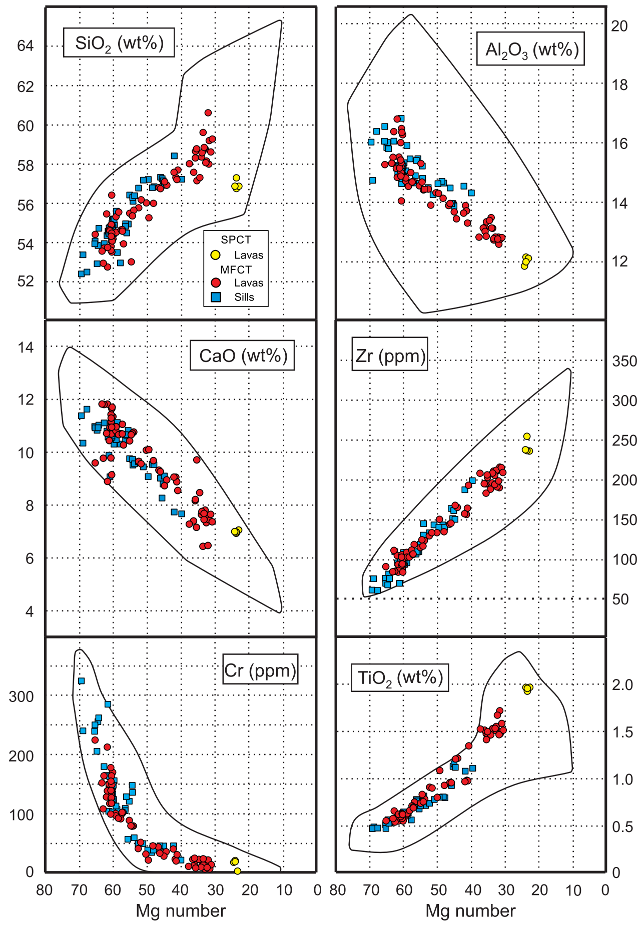

Fig. 11. Variation diagrams for selected major and trace elements v. Mg# for Ferrar Group lavas and sills to illustrate the geochemical coherence of the MFCT and the restricted and different composition of the SPCT. Plotted data include only fine-grained samples of lavas and chilled margins of sills from north Victoria Land, south Victoria Land and the central Transantarctic Mountains. Data sources: Elliot and Fleming (2017) and unpublished data. The outlined fields reflect data published in the literature over a period of more than 50 years, and which are compiled in the GEOROC database (Sarbas *et al.* 2017). The greater dispersion in those data is attributed to a combination of analytical issues, alteration and *in situ* differentiation in some larger magma bodies. Analyses reflecting cumulate compositions have been removed but it is more difficult to identify samples affected by *in situ* differentiation at the evolved end of the compositional spectrum (Mg# <30).

have Mg# = 40–65, and in north Victoria Land the Mesa Range lavas have a relatively restricted range of Mg# = 50–62. Excluding the olivine-bearing dolerites sills, chilled margins of sills in the Shackleton Glacier region have a Mg# range of 45–65, and in the Queen Alexandra Range region the range in Mg# is 56–65, which is in contrast to the lavas (Mg# <45). In south Victoria Land, the sills in the Dry Valleys have a Mg# range of 40–60, and in the Prince Albert Mountains the Mg# range is 55–62. In north Victoria Land the Mg# of the sills lies in the range 48–62. There is no spatial pattern in the geochemistry of the sills, but quite clearly the opposite is the case for the lavas and implies the eruption of regionally distinct batches of magma. This probably reflects differing residence times in crustal magma chambers prior to supracrustal emplacement. Further, it suggests the sills might be an episode of magma emplacement distinct from that of the extrusive rocks.

Isotope geochemistry

The unusually high initial Sr isotope composition of Ferrar tholeiites (Sr_i *c.* 0.711) from the Dry Valleys region of south Victoria Land was established by Compston *et al.* (1968), following on from investigation of the Tasmanian dolerites by Heier *et al.* (1965). These early results for the Ferrar dolerites were extended to the Kirkpatrick Basalt lavas in the Queen Alexandra Range (Table 4: all Sr and Nd isotope data have been recalculated to an age of 182.7 Ma), and the Sr isotope compositions (Sr_i = 0.7094–0.7133) were related to large-scale contamination of basaltic magma by granitic rocks (Faure *et al.* 1972, 1974, 1982).

Subsequent oxygen isotope studies on whole-rock lavas from all major outcrop regions (Hoefs *et al.* 1980; Kyle *et al.* 1983; Mensing *et al.* 1984, 1991) found a wide range of $\delta^{18}O$ values (6.0–9.3), and the weak correlations with initial $^{87}Sr/^{86}Sr$ were interpreted to support crustal assimilation. Later work (Fleming *et al.* 1992) revealed that much of the range of whole-rock oxygen isotope compositions could be found in a single chemically homogeneous lava flow ($\delta^{18}O$ = 5.8–8.1), with the plagioclase separates from that flow having a markedly limited range ($\delta^{18}O$ = 5.5–5.8), which approaches mantle-like values. The large range of previously published whole-rock compositions was reinterpreted to be the result of low-temperature interaction (alteration) of fine-grained and glassy components in the rocks with meteoric water. The Sr–O variations in the chilled margins of

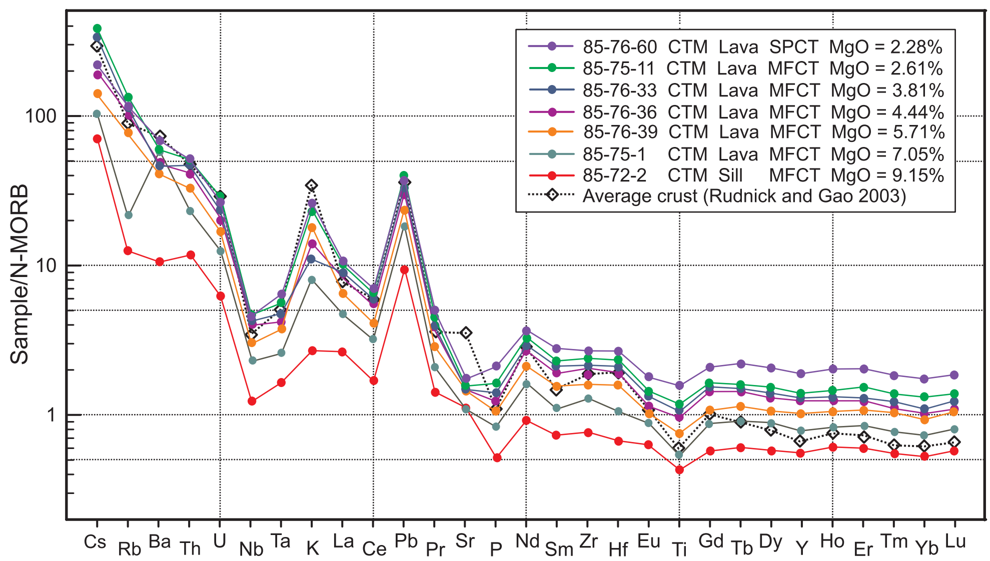

Fig. 12. MORB-normalized trace element diagram for samples (from Dawson Peak and Storm Peak) of the Ferrar Group selected to cover the entire range of MgO concentrations observed. The normalization factors are from Sun and McDonough (1989). Data source: Table 4 and Elliot and Fleming (2017 and supplementary data therein).

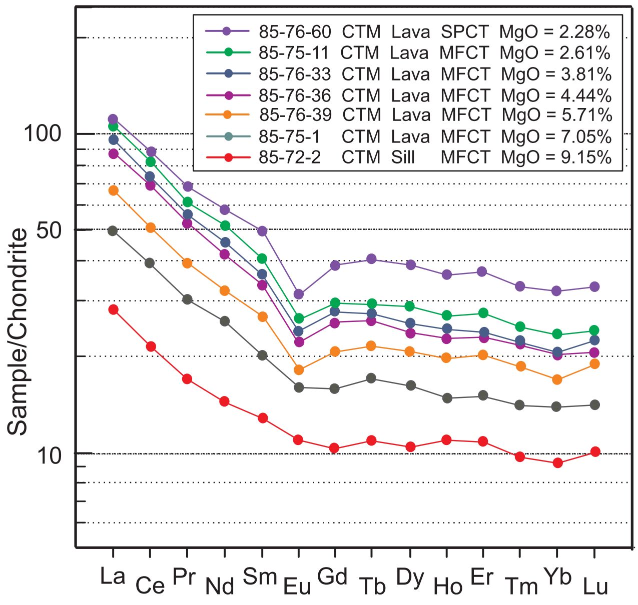

Fig. 13. Chondrite-normalized rare earth element diagram for Ferrar Group samples (from Dawson Peak and Storm Peak) illustrated in Figure 12. The normalization factors are from Sun and McDonough (1989).

Tasmanian sills and the sill at Portal Rock had also been interpreted as the result of meteoric water interactions (Hergt *et al.* 1989*a*, *b*). In contrast to the extrusive rocks, sills have been shown to have a range of compositions that trend towards very low values ($\delta^{18}O = 1.9–6.1$) (Hergt *et al.* 1989*b*; Faure *et al.* 1991). For the Dufek intrusion, whole-rock $\delta^{18}O$ values for the lower section in the Dufek Massif are 5.0–6.9, but the Forrestal Range upper section is much more varied and $\delta^{18}O$ values lie between 0.0 and 6.1 (Kistler *et al.* 2000). The mineral data are equally skewed, with Dufek plagioclase ($\delta^{18}O = 6.2–7.7$) and pyroxene ($\delta^{18}O = 4.6–5.3$) differing from Forrestal plagioclase ($\delta^{18}O = 0.3–6.4$) and pyroxene ($\delta^{18}O = 2.1–5.6$). These trends towards lower $\delta^{18}O$ values in intrusive rocks have been attributed to interactions with meteoric water at high temperatures and provide evidence for large-scale hydrothermal systems operating at the time of emplacement.

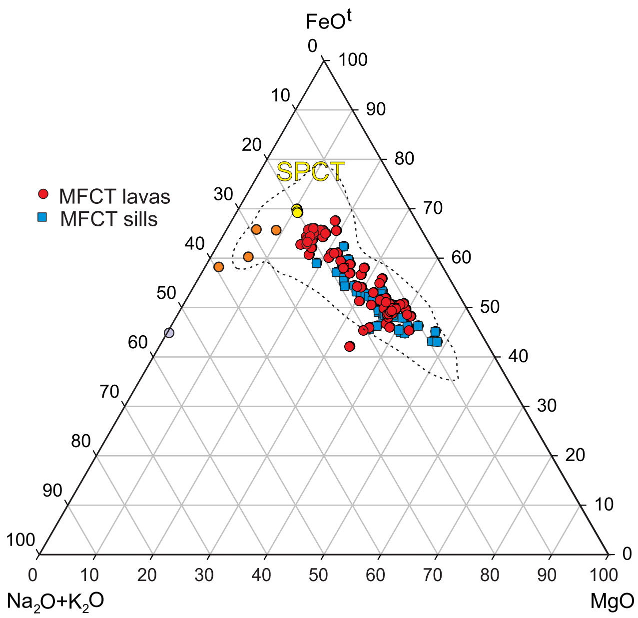

Fig. 14. Compositions of Ferrar rocks (MFCT and SPCT) on an AFM diagram ($Na_2O + K_2O–FeO^T–MgO$, where FeO^T = Fe total as FeO) illustrating the Fe-enrichment trend of the MFCT and the Fe-rich SPCT composition. Data sources: Elliot and Fleming (2017 and supplementary data therein); evolved compositions from Melluso *et al.* (2014) are in orange, and an interstitial glass from Elliot *et al.* (1995) is in pale blue. The field for the Ferrar province as a whole is from the GEOROC database (Sarbas *et al.* 2017).

Thus, the oxygen isotope trends (Fig. 15) predominantly reflect the operation of two different processes: (1) interaction with high-temperature waters causing a decrease in $\delta^{18}O$; and (2) alteration at low temperatures causing an increase in $\delta^{18}O$. The extrusive rocks are more widely affected by the low-temperature process because their glassy textures are more susceptible to alteration. The intrusive rocks are affected more by the high-temperature process because their protracted cooling allows for more extended high-temperature water–rock interactions. Further, because they are holocrystalline they tend to be less susceptible to low-temperature alteration. Nevertheless, the existing mineral data suggest that there is a small increase in $\delta^{18}O$ (<1%) which is largely masked by other more dominant processes, but is attributable to assimilation.

Despite the complications in the oxygen isotope system and the near-mantle $\delta^{18}O$ for the least altered minerals, the broad correlation between initial Sr isotope composition and MFCT whole-rock chemistry (Fig. 16) demonstrates that a component of crustal assimilation is important in the evolution of these rocks. The SPCT lavas fall at the end of a different and more extended evolutionary path, which must have involved considerably less assimilation.

An initial Sr isotope ratio of 0.70808, calculated by means of an Rb/Sr isochron for a sill at Mount Achernar in the central Transantarctic Mountains (Faure *et al.* 1991) and the lowest for a Ferrar sill or lava (excluding the Dufek intrusion), is here confirmed for the chilled margin of that sill (Table 5). The range in Sr isotope initial ratios for Ferrar rocks in the Ross Sea sector varies between 0.70710 and 0.71381 (Table 5), which is the result of secondary processes, as well as crustal assimilation. In the Weddell Sea sector, elevated initial Sr isotope ratios (Sr_i >0.710) were reported by Ford and Kistler (1980) for the Pecora Escarpment (Fig. 1), and by Brewer *et al.* (1992) and Leat (2008) for the Whichaway Nunataks and Theron Mountains (Sr_i >0.70819). The Dufek intrusion (including the capping granophyre) has an initial Sr isotope ratio range for whole-rock analyses of 0.70830–0.71541 (Ford *et al.* 1986; Kistler *et al.* 2000) but with pyroxene as low as 0.70763. Mukasa *et al.* (2003) reported a wider range of preliminary data for plagioclase and pyroxene (Sr_i = 0.70609–0.71656). At the other end of the province, the Kirwans Dolerite in New Zealand (Mortimer *et al.* 1995) has Sr_i of 0.71023–0.71073.

In contrast to the earlier proposed contamination model, Kyle (1980) and Kyle *et al.* (1983) favoured a mantle origin for the high baseline Sr isotope initial ratios, but with a degree of superimposed crustal contamination to explain the range in Sr and O isotope values. The first Nd isotope measurements (Tasmanian dolerite: ε_{Nd} *c.* – 5.1) for the Ferrar province (Table 4) were published by Hergt *et al.* (1989*a*, *b*), who also argued for a mantle origin for the isotope and other geochemical characteristics. Fleming *et al.* (1995) showed that a correlation exists between ε_{Nd} and Sr_i (Fig. 17; Table 5), and that it is consistent with the well-constrained variation observed in the major and trace element compositions of the MFCT tholeiites (Fig. 11). This isotope correlation extends to the olivine-bearing dolerites (Elliot and Fleming 2017), which are the least-evolved of all Ferrar rocks and yields the range ε_{Nd} *c.* −3.80 and Sr_i *c.* 0.70878 to ε_{Nd} *c.* −5.95 and Sr_i *c.* 0.71288 for the best-constrained analyses (the total

Table 4. *Summary of Nd , Sr and O isotope data for Ferrar Large Igneous Province tholeiites*

Region	Location	Chemical type	ε_{Nd}	Sr_i	$\delta^{18}O$	Reference
Tasmania		MFCT wr sill*	−6.6 to −5.1	0.70934–0.71278	1.9–6.1	Hergt *et al.* (1989*b*)
New Zealand	Reefton	MFCT wr sill	−5.6 to −5.3	0.71023–0.71073		Mortimer *et al.* (1995)
North Victoria Land	Mesa Range	SPCT wr lavas		0.70863–0.70957	5.5–8.2	Fleming *et al.* (1992)
		SPCT wr lavas	−4.4 to −4.2	0.70858–0.70958		Fleming *et al.* (1995)
		MFCT wr lavas	−5.5 to −4.8	0.70872–0.71160		
		MFCT pyx.	−5.4	0.70951–0.70955		
		MFCT plag.		0.71061		
		SPCT wr lavas	−4.4 to −4.1	0.70954–0.70968		Elliot *et al.* (1999)
		SPCT plag.		0.70952		
	Thern Promontory	MFCT wr sill†	−5.9 to −5.1	0.71141–0.71304		Brotzu *et al.* (1992)
South Victoria Land	Prince Albert Mountains	MFCT wr sills, lavas	−5.6 to −3.3	0.71015–0.71198	4.8–8.0	Molzahn *et al.* (1996)
		MFCT pyx.	−5.3 to −4.4	0.70955–0.71201	5.2–6.2	
		MFCT plag.	−5.6 to −3.0	0.70763–0.71360	6.0–13.3	
		SPCT wr lavas	−3.5	0.70948	6	
		SPCT pyx.		0.70987	5.2	
		SPCT plag.		0.70987	18.3	
	Prince Albert Mountains	MFCT wr lavas†	−5.7 to −4.7	0.71028–0.71213		Antonini *et al.* (1999)
		SPCT wr lava	−3.8 to −3.3	0.70938–0.70973		
	Prince Albert Mountains	MFCT wr lavas	−5.4 to −5.1	0.70959–0.71381		Fleming (unpublished data)
	Prince Albert Mountains	SPCT wr lava	−4.4 to −4.3	0.70903–0.70929		Elliot *et al.* (1999)
		SPCT plag.		0.70949		
	Prince Albert Mountains	MFCT wr lavas		0.7098–7115	6.2–8.3	Kyle *et al.* (1983)
	Carapace Nunatak	MFCT wr lavas	−5.6 to −5.2	0.71063–0.71127		Fleming *et al.* (1998)
	Dry Valleys	MFCT wr sills	−5.7 to −5.2	0.71054–0.71191		
	Roadend Nunatak	MFCT wr sills		0.7091–0.7152	4.7–7.1	Faure *et al.* (1991)
Central Transantarctic Mountains	Storm Peak	MFCT wr lavas	−6.0 to −4.6	0.70970–0.71289		Fleming (1995)
		MFCT pyx.	−5.5 to −4.9	0.70982–0.71273	6.1–6.6	
		MFCT plag.		0.71024–0.71283	6.4–6.8	
		SPCT wr lava	−4.3 to −4.2	0.70957–0.70968		
		SPCT pyx.	−4.3 to −4.2	0.70962–0.71269	6.9	
		SPCT plag.		0.70963–0.70970	5.3–5.9	
	Dawson Peak	MFCT wr sill	−4.1 to −3.9	0.70987–0.71009		
		MFCT Ol-dol sill	−4.0 to −3.7	0.70768–0.70869		
		MFCT Ol-dol. plag		0.70877		
	Mount Achernar	MFCT wr sills		0.70710–0.71027	4.4–6.5	Faure *et al.* (1991)
	Queen Alexandra Range	MFCT wr sills	−5.4 to −3.8	0.70808–0.71264		Fleming (unpublished data)
	Portal Rock	MFCT wr sill‡	−6.0 to −5.2	0.70901–0.71082	1.9–6.1	Hergt *et al.* (1989*a*)
	Shackleton Glacier region	MFCT wr sills	−5.4 to −4.5	0.70859–0.71139		Fleming (unpublished data)
	Storm Peak	SPCT wr lavas	−4.3 to −4.2	0.70945–0.70949		Elliot *et al.* (1999)
	Grosvenor Mountains	SPCT wr lavas	−4.4 to −4.3	0.70946–0.70947		
	Nilsen Plateau	MFCT wr sills	−5.4 to −3.9	0.70971–0.71368		Fleming (unpublished data)
Theron Mountains		MFCT wr sills†	−5.0 to −3.7	0.70817–0.70955		Leat *et al.* (2006)
		SPCT wr sill†	−3.9 to −3.8	0.70878–0.70992		
Dufek Intrusion	Dufek Massif	MFCT wr		0.70828–0.71486	5.0–6.9	Kistler *et al.* (2000)
		MFCT pyx.		0.70743–0.70912	4.6–5.3	
		MFCT plag.		0.70896–0.70984	6.2–7.7	
	Forrestal Range	MFCT wr		0.70874–0.71200	0.1–6.2	
		MFCT pyx.		0.70816–0.71172	3.2–4.1	
		MFCT plag.		0.70932–0.71244	3.2–5.4	
	Dufek Massif	MFCT wr†		0.70609–0.71656		Mukasa *et al.* (2003)

Plag., plagioclase; pyx., pyroxene; wr, whole rock. Sr and Nd data are calculated to an age of 182.7 Ma.
*Hergt *et al.* (1989*a*, *b*) data renormalized to $^{146}Nd/^{144}Nd = 0.7219$ and adjusted to LaJolla Nd standard $^{143}Nd/^{144}Nd = 0.511843$.
†Data as reported.
‡Nd measurements at lower resolution and as reported.

range for all Ferrar province analysed samples, excluding the Dufek intrusion, is slightly greater: ε_{Nd} *c.* −3.0 to 6.6 and Sr_i *c.* 0.70710–0.71381). The SPCT rocks have highly evolved major and trace element compositions, but isotopically are closer to the olivine-bearing dolerites.

Unfortunately, there are no published Nd isotope data to complement the low Sr_i of pyroxene in the Dufek intrusion other than a reported initial Nd isotope ratio range of 0.51213–0.51233 for plagioclase and pyroxene (Mukasa *et al.* 2003). It should be noted that the full range of reported initial Sr and Nd isotope compositions is greater than that in Figure 17, and, as already noted, it is attributed to analysis in different laboratories at different times, and alteration effects.

There are few Pb isotope analyses for the Ferrar province as a whole. Hergt *et al.* (1989*b*), Mortimer *et al.* (1995) and Antonini *et al.* (1999) analysed whole-rock samples and provided initial ratio data (cf. Brewer *et al.* 1992; Kyle *et al.* 1987), whereas Molzahn *et al.* (1996) and Mukasa *et al.* (2003) analysed plagioclase, which requires little or no correction for *in situ* U and Th decay. The $^{207}Pb/^{204}Pb$ initial ratios of whole rocks and of plagioclase lie in the range 15.61–15.68, with

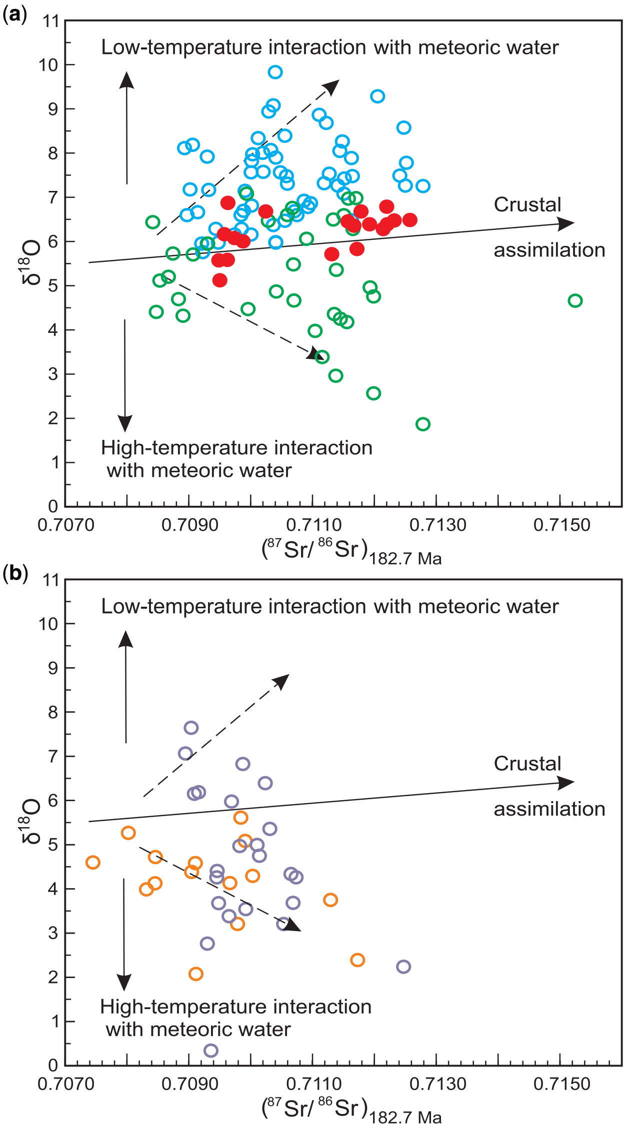

Fig. 15. ^{87}Sr/^{87}Sr$_i$ (at 182.7 Ma) v. δ^{18}O for Ferrar province rocks and minerals throughout the Transantarctic Mountains. (**a**) Whole-rock Kirkpatrick Basalt lavas (blue circles), Ferrar Dolerite sills (green circles), and pyroxene and plagioclase (red circles). See Table 4 for the data sources. (**b**) Pyroxene (orange circles) and plagioclase (purple circles) data for the Dufek intrusion (Kistler *et al.* 2000). Dashed arrows represent diagrammatic paths of evolution depending on high- or low-temperature alteration.

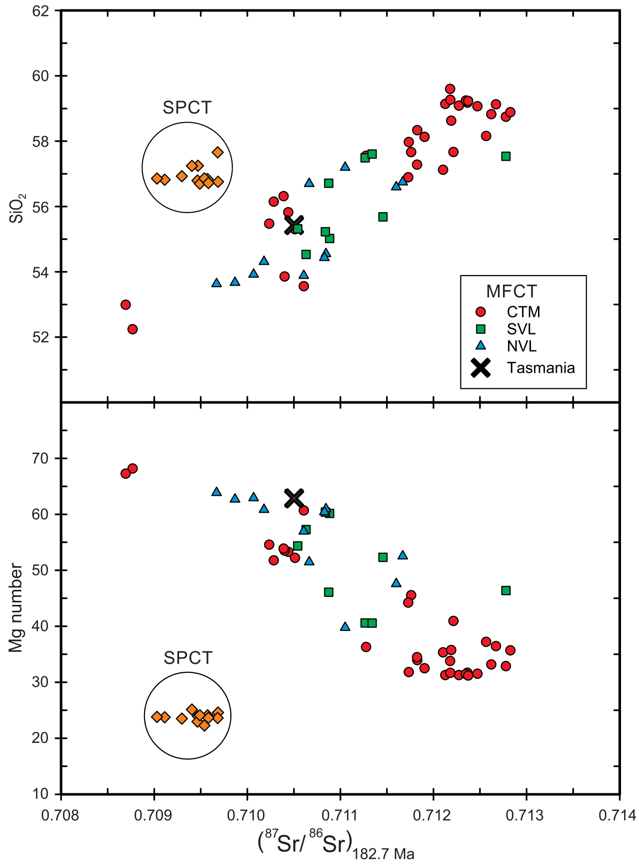

Fig. 16. ^{87}Sr/^{87}Sr$_i$ (at 182.7 Ma) v. SiO$_2$ and Mg number, illustrating MFCT correlations that reflect fractional crystallization and crustal assimilation. Data points represent the Ferrar province from north Victoria Land to the central Transantarctic Mountains. The SPCT composition must have followed a different evolutionary path. Data sources are the same as for Figures 11 and 15.

^{208}Pb/^{204}Pb ratios of 38.24–38.54 and ^{206}Pb/^{204}Pb ratios of 18.55–18.64. These ratios, plotting above the Northern Hemisphere Reference Line, reflect the high abundance of Pb and its crustal character. Osmium isotopes also have been measured (Molzahn *et al.* 1996; Brauns *et al.* 2000; Hergt and Brauns 2001; Mukasa *et al.* 2003). Os concentrations are quite low, leading to significant uncertainties, but initial ratios are consistent with a mantle origin (^{187}Os/^{188}Os$_i$ = 0.145 ± 0.049–0.194 ± 0.023). This has been confirmed by a detailed investigation of the Basement Sill in south Victoria Land (Choi *et al.* 2019*a*), which reported subchondritic Os/Ir ratios (<0.33) and a least radiogenic value of ^{187}Os/^{188}Os = 0.1609 ± 0.0003 (2σ), although the total range is quite extended (up to ^{187}Os/^{188}Os$_i$ = 8.100 ± 1.600).

Mensing *et al.* (1984, 1991) reported variable sulfur isotope compositions for Mesa Range tholeiites, which were attributed to outgassing under a range of oxygen fugacities; a conclusion also reached for the Kirkpatrick Basalt at Mount Falla, Queen Alexandra Range (Faure *et al.* 1984). Low sulfur saturation has been proposed to account for the PGE abundances in MFCT sills in north Victoria Land (Hanemann and Viereck-Götte 2007*a*).

Several conclusions have been drawn from these results. First, Ferrar rocks have high initial strontium isotope ratios, which begin at a baseline value of 0.708 (with the majority >0.709), and low ε_{Nd} values (most are more negative than −3.7). Second, mineral separates confirm that both high and low whole-rock δ^{18}O values result from secondary processes. Third, there is a clear correlation between Sr and Nd isotope ratios, which, together with the whole-rock chemistry, points to a path of low-pressure evolution involving both fractional crystallization and assimilation of crustal material, from olivine-bearing dolerite to andesitic compositions.

Post-emplacement alteration and secondary mineralization

Fleming *et al.* (1989, 1992, 1993) proposed a mid-Cretaceous alteration event affecting the Kirkpatrick Basalt lavas based on a 103 Ma Rb/Sr array or 'errorchron' derived from SPCT samples. They attributed it to tectonism related to the break-up of Antarctica and Australia, and the development of associated hydrothermal systems, which caused mobility of Rb. This event is reflected by scattered K/Ar dates and anomalous palaeomagnetic pole positions determined for the lavas

Table 5. *MgO%, Rb, Sr, Sm and Nd concentrations, and $^{87}Sr/^{86}Sr$ and $^{143}Nd/^{144}Nd$ present-day and calculated initial ratios for selected tholeiites*

Sample	MgO %	Rb (ppm)	Sr (ppm)	$^{87}Rb/^{86}Sr$	$^{87}Sr/^{86}Sr^{*}$	$^{87}Sr/^{86}Sr^{\dagger}$	$\varepsilon_{Sr}^{\ddagger}$	Sm (ppm)	Nd (ppm)	$^{147}Sm/^{144}Nd$	$^{143}Nd/^{144}Nd^{*}$	$^{143}Nd/^{144}Nd^{\dagger}$	$\varepsilon_{Nd}^{\ddagger}$
85-72-2	9.14	6.3	115.6	0.1575	0.709173(10)	0.708764(10)	60.8	1.85	7.4	0.1510	0.512381(5)	0.512200(5)	−3.95
85-75-1	6.99	10.5	100.2	0.3044	0.711421(10)	0.710630(11)	87.3	2.94	12.4	0.1432	0.512310(6)	0.512139(6)	−5.16
85-76-42	6.15	41.5	123.0	0.9772	0.712707(10)	0.719169(16)	80.7	3.63	15.4	0.1423	0.512330(7)	0.512160(7)	−4.74
85-76-39	5.67	44.6	131.1	0.9792	0.713053(11)	0.710509(17)	85.6	4.03	17.1	0.1425	0.512317(7)	0.512147(7)	−5.00
85-76-36	4.44	57.4	136.3	1.2201	0.714786(9)	0.711617(19)	101.3	4.95	21.8	0.1374	0.512289(6)	0.512125(6)	−5.43
85-76-33	3.80	65.9	136.3	1.3991	0.715539(14)	0.711905(23)	105.4	5.30	23.5	0.1365	0.512277(6)	0.512114(6)	−5.64
85-76-20	3.26	74.1	139.0	1.5431	0.715782(9)	0.711773(23)	103.5	5.79	25.6	0.1367	0.512274(5)	0.512111(5)	−5.71
85-76-17	3.25	56.9	64.3	2.5632	0.717934(9)	0.711276(36)	96.5	5.82	26.1	0.1349	0.512284(6)	0.512123(6)	−5.47
85-76-29	3.18	61.5	131.9	1.3493	0.716273(8)	0.712768(20)	117.7	5.84	26.1	0.1352	0.512270(5)	0.512108(50	−5.75
85-76-49	2.89	73.4	134.2	1.5841	0.715850(9)	0.711735(23)	103.0	6.22	27.5	0.1364	0.512286(4)	0.512123(4)	−5.46
85-76-23	2.88	67.2	142.9	1.3630	0.716161(9)	0.712740(40)	117.2	5.83	26.1	0.1352	0.512265(7)	0.512109(7)	−5.89
85-75-11	2.58	76.8	137.6	1.5946	0.716270(10)	0.712128(24)	108.6	5.83	26.0	0.1355	0.512271(6)	0.512109(6)	−5.74
85-76-60	2.26	66.7	128.8	1.4979	0.713460(9)	0.709569(22)	72.2	7.42	31.3	0.1435	0.512353(6)	0.512181(6)	−4.32
11-1-3	6.03	22.8	169.5	0.3885	0.709088(9)	0.708078(10)	48.2	3.17	13.8	0.1395	0.512344(7)	0.512177(7)	−4.41

*Present-day measured isotopic ratios normalized with $^{87}Sr/^{86}Sr = 0/119400$ or $^{143}Nd/^{144}Nd = 0.721900$. 2σ mean within-run uncertainties in the last digits are given in parentheses. Mean values (and 1σ external reproducibilities) for standards measured during the same period are: SRM 987, $^{87}Sr/^{86}Sr = 0.710243$ (±0.000010); and LaJolla Nd, $^{143}Nd/^{144}Nd = 511843$ (±0.000005).

†Calculated model initial ratios at 182.7 Ma with decay constants of 1.42×10^{-11} (^{87}Rb) or 6.54×10^{-12} (^{147}Sm); uncertainties (in parentheses) provide for uncertainties in present-day measured isotopic ratios, parent/daughter ratios (0.5% for $^{87}Rb/^{86}Sr$ and 0.1% for $^{147}Sm/^{144}Nd$) and age (±1.8 Ma).

‡Conventional ε notation for 182.7 Ma with reference values of $^{87}Rb/^{86}Sr = 0.085$, $^{87}Sr/^{86}Sr = 0.7047$, $^{147}Sm/^{144}Nd = 0.1966$ and $^{143}Nd/^{144}Nd = 0.512638$.

Samples were selected to illustrate the range of MgO contents and isotopic compositions in a single relatively restricted region. Ferrar tholeiites from the central Transantarctic Mountains: olivine-bearing dolerite (85-72-2) with the highest MgO content of all sills and lavas from near Dawson Peak; lavas from Peterson Ridge near Storm Peak (see also Table 3); and the sill (11-1-3), with the lowest Sr isotope initial ratio recorded for any lava or sill, from near Mount Achernar. Data are from Fleming (1995) and previously unpublished data (sample 11-1-3). Grid references are given in Appendix A.

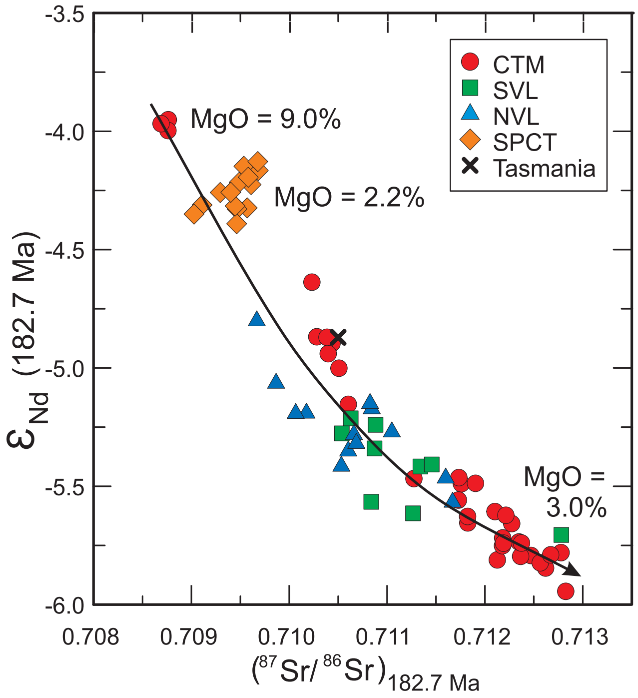

Fig. 17. ε_{Nd} v. $^{87}Sr/^{87}Sr_i$ (at 182.7 Ma) for Ferrar Large Igneous Province sills and lavas from north Victoria Land to the central Transantarctic Mountains. Data sources: for Tasmania, Hergt *et al.* (1989*b*); for Antarctica, Fleming (1995), Fleming *et al.* (1992, 1995) and Elliot *et al.* (1999); and unpublished data for south Victoria Land. Other data are not plotted: (1) because of analytical uncertainties (not given, large or highly variable) and interlaboratory biases; and (2) because whole-rock $^{87}Sr/^{87}Sr$ ratios for sill margins are affected by high-temperature alteration and, lacking measurement of Sr isotope ratios for plagioclase in the same rock, are subject to uncertainties.

(McIntosh *et al.* 1986; Delisle and Fromm 1989; Faure and Mensing 1993; Mensing and Faure 1996). Molzahn *et al.* (1999) dated apophyllite from vugs in the Kirkpatrick Basalt in the Prince Albert Mountains by the $^{40}Ar/^{39}Ar$ method and determined a crystallization age of 96.7 ± 0.6 Ma, which they interpreted in terms of an alteration event. A less well-defined apophylllite crystallization event was dated at 125–112 Ma. Age determinations of apophyllites by the $^{40}Ar/^{39}Ar$ and Rb/Sr methods (Fleming *et al.* 1999) extended those earlier results. Total $^{40}Ar/^{39}Ar$ gas ages vary from 133 to 114 Ma for the Queen Alexandra Range, 114–95 Ma for south Victoria Land and 100–76 Ma for north Victoria Land. Rb/Sr model ages range from 144 to 94 Ma; in some instances ages are concordant with the Ar total gas ages and in others are as much as 14 myr older. These data have been interpreted to record the early stage of uplift of the Transantarctic Mountains (Fleming *et al.* 1999). The differing patterns of age were attributed to the mountain range consisting of several major blocks which had different uplift histories (Fitzgerald 2002), let alone differing hydrological systems and thermal regimes. Further, the youngest apophyllite ages are broadly comparable to that of the metamorphic core complex in Marie Byrd Land (about 105 Ma), which marks separation of the New Zealand microcontinent from West Antarctica (Siddoway 2007) and the initiation of the West Antarctic Rift System.

The zeolite assemblage in the lava successions (see Elliot *et al.* 2021) suggests the possibility of a now eroded overburden of Ferrar lavas and/or Mesozoic sedimentary strata 1 km or more thick. Rather than recording the early stages of uplift, Lisker and Läufer (2013) have argued that a Jurassic–early Cretaceous sedimentary basin, overlying the Ferrar lavas but now eroded, better explains the apatite fission-track uplift data for the Transantarctic Mountains. A variety of thermal regimes and hydrological systems would also have existed in and beneath such a basin, thus leading to secondary mineralization and young Ar ages for lavas, and Cretaceous ages for apophyllites.

Magma emplacement at supracrustal depths and evolution

Building on the early work of Gunn (1962, 1966) on the sills in the Dry Valleys region, investigation of the Basement Sill has provided fundamental information on the mode of emplacement at upper-crustal depths (low pressure) and subsequent textural evolution of basic magmas (Bédard *et al.* 2007; Charrier 2010; Jerram *et al.* 2010; Charrier and Manochehri 2013; Petford and Mirhadizadeh 2017). The Basement Sill, which has been identified over an area of about 10 000 km^2 (Marsh 2007), is interpreted to be the result of injection of large batches of magma with an entrained tongue of orthopyroxene. Magmas spread outwards, as a series of lobes, from an inferred point of origin, which is postulated to be a vertical conduit connected at depth to the magma source (Marsh *et al.* 2005; Souter *et al.* 2006). The relatively fast cooling of the sill resulted in preservation of compaction and interstitial liquid segregation features, which are generally lost in more slowly cooled and thoroughly annealed layered basic intrusions (e.g. Dufek intrusion). Comparable injection of magma batches has also been proposed for the Beacon (Asgard) Sill in the Dry Valleys (Zieg and Marsh 2012). With this as a model, sills elsewhere may be interpreted as lateral injections principally into Beacon strata, and possibly from at least three principal centres spaced along the Transantarctic Mountains (Elliot and Fleming 2008). Based on their modelling results for the Basement Sill, Petford and Mirhadizadeh (2017) estimated lateral emplacement times. Assuming a constant viscosity of 33 Pa s, together with continuous and uniform flow in chemically coherent magma, lateral transport over 3000 km could be accomplished in about 1 year. At higher viscosities (e.g. 10^4 Pa s) a similar distance would take less than 2×10^5 years. Further, they estimated that the Basement Sill could have been filled in 10^5 years, provided viscosity and supply rate remained constant.

Ongoing studies of the mode of emplacement and accumulation in the lower part of the Dufek intrusion have been reported by Cheadle *et al.* (2007), Grimes *et al.* (2008), Carnes *et al.* (2011) and Gee *et al.* (2013). They suggest multiple magma injection events, as recorded by xenolith-rich layers and sharp contacts between modal units. Cheadle and Gee (2017) reported studies on mineral orientation and magnetic data aimed at assessing the physical processes operating in the development of cumulate rocks.

In situ geochemical evolution of magmas in sills is by fractional crystallization, with evidence for segregation of interstitial liquids shown in vertical pipes and schlieren of more evolved compositions (e.g. Zavala *et al.* 2011). Plagioclase cumulates, accompanied by migration of differentiates away from the site, were noted by Hergt *et al.* (1989*a*) for the Portal Rock sill in the Queen Alexandra Range.

The compositions of chilled margins of sills and fine-grained lavas reflect varying degrees of evolution of basic magmas (MgO *c.* 9%) at crustal depths by fractional crystallization (pyroxene–plagioclase–oxide) together with minor crustal assimilation (Menzies and Kyle 1990; Fleming 1995; Fleming *et al.* 1995; Antonini *et al.* 1999). The majority of the lavas are basaltic andesite and andesite in composition, but range from basalt to dacite (but to dacite only if the evolved Thern Promontory rocks are lavas and not evolved portions of sills, and discounting the contaminated Butcher Ridge rocks). Interstitial glass and minerals demonstrate the continued evolution at low pressures of dry tholeiitic magmas to silicic compositions with the crystallization of ferrohedenbergite, fayalite, quartz, alkali feldspar and a variety of trace minerals (e.g. monazite, allanite) (Melluso *et al.* 2014).

The Butcher Ridge igneous complex (Fig. 1) (Marshak *et al.* 1981; Shellhorn 1982; Kyle *et al.* 1999; Nelson *et al.* 2014) comprises rocks ranging from basalt to rhyolite, but the evolved components (high-K andesite to high-K rhyolite compositions) are interpreted to be the result of interaction with crustal materials, not the evolution of a magmatic system by simple fractional crystallization. Analysis of the vitrophyric rocks shows a high water content, and widespread hydration by snow- and ice-derived water (Nelson *et al.* 2018).

Separation, on the Sr–Nd isotope correlation diagram, of the olivine-bearing dolerites from the rest of the MFCT rocks suggests that they might form a separate but related intrusive event, in the same sense as that of the SPCT. The distinctive lava compositions from north Victoria Land (uniformly high MgO) compared with south Victoria Land (moderate MgO) and the Queen Alexandra Range and Grosvenor Mountains (almost uniformly low MgO) also suggest magma pulses and differing extents of evolution before eruption (the precision of age determinations does not yet allow a temporal evaluation of this possibility). Despite the strong correlation between Nd and Sr isotope compositions (Fig. 17), the Mg number, as an indicator of evolution, does not correlate quite as well with isotopic evolution. This may result from fractionation before and/or after crustal input, and indicates more complex evolutionary paths resulting from differing crustal-level residence times and episodic assimilation of crustal materials. These complexities are illustrated by the lavas at Storm Peak (Table 5) for which decreasing MgO is not accompanied by smoothly changing initial isotope ratios of strontium and ε_{Nd} values.

Origin

The geochemical characteristics of the Ferrar rocks, specifically the enriched initial isotope ratios of Sr, Nd and Pb but also mantle-like $\delta^{18}O$ and Os isotopes plus the low HFSE abundances (particularly Ti) and crust-like trace element patterns even in the most basic olivine-bearing dolerites (MgO *c.* 9%), have posed major questions for the understanding of the origin of the primary magmas in the mantle and their subsequent evolution to the least-evolved Ferrar rock. The presence of forsteritic olivine (Fo_{88}) in the olivine-bearing dolerites is consistent with equilibrium with the mantle, and the absence of a Eu anomaly indicates that the chemical composition of these most basic Ferrar rocks was little affected by low-pressure processes. Superimposed on this are the crustal evolution of the MFCT olivine-bearing dolerite composition to the most-evolved andesitic composition, and also the evolution of the primary magma to yield the SPCT magma type, which is highly evolved geochemically but, compared with the MFCT, less evolved isotopically.

The most distinctive characteristic of the SPCT, apart from its restricted composition, is evident in Figure 17, which shows the lack of isotopic evolution relative to the evolved MFCT rocks. In all other geochemical characteristics, it is similar to the MFCT and thus a Ferrar magma type. Fleming *et al.* (1995) suggested that it could have been derived from an olivine-bearing dolerite composition by fractional crystallization but with only very limited assimilation of crustal material. A similar conclusion was also reached by Antonini *et al.* (1999). In contrast, Brotzu *et al.* (1992) suggested the relatively evolved tholeiites of the Thern Promontory and Archambault Ridge (Fig. 8) provided a link between the low-TiO_2 (MFCT) and high-TiO_2 (SPCT) rocks, although the Sr and Nd isotope data (Fig. 17) render this proposal most improbable. On the other hand, experimental studies by Hanemann and Viereck-Götte (2007*b*) suggested that the major and trace element differences can be attributed to different oxygen fugacities, activities of water and depths of magma evolution. In their model, the MFCT and SPCT rocks were generated from the same source but the former evolved at greater depths in the crust with higher oxygen fugacity (f_{O_2}) and activity of water (a_{H_2O}), and the latter at shallower crustal depths with lower f_{O_2} and a_{H_2O}. It should be noted that emplacement of the SPCT lavas and sills is a post-MFCT late-stage short-lived event in the Ferrar province.

A mantle origin for the geochemical characteristics, as opposed to crustal contamination of either basaltic magmas or an isotopically depleted mantle source, was first proposed by Kyle (1980), and later attributed to a source in the subcontinental mantle lithosphere enriched by crustal materials (Kyle *et al.* 1983). Hergt *et al.* (1989*b*), in a study of the Tasmanian dolerites, evaluated the lithospheric source proposal and pointed out that crustal contamination of mid-ocean ridge basalt (MORB), oceanic island basalt (OIB) and island arc tholeiite (IAT) type parental magmas is incompatible with the geochemistry of those tholeiites (which are part of the Ferrar province). Rather, the mantle source had assimilated a small proportion (<3%) of subducted sediment, thus giving enriched mantle characteristics somewhat similar to enriched MORB (i.e. E-MORB). Menzies and Kyle (1990) reviewed the possible alternative sites of generation in the lithosphere and/or the asthenosphere and advocated a Dupal-like mantle with $^{87}Sr/^{86}Sr = 0.704–0.707$ and a strong subduction zone signature suggesting crustal recycling. Fleming *et al.* (1995) proposed a somewhat different process, which involved a depleted mantle contaminated with Paleozoic-age crustal materials either by sediment subduction, tectonic erosion of continental crust or delamination of lower crustal materials. Partial melting followed by a melting–assimilation–storage–homogenization (MASH) process (Hildreth and Moorbath 1988) was proposed as the path to yield the most primitive Ferrar magmas, followed by assimilation–fractional crystallization processes in the upper crust to explain the observed range in isotopic and geochemical compositions. On the basis of isotope and trace element data, Molzahn *et al.* (1996) considered the Ferrar source to be subcontinental mantle lithosphere modified by crustal material. Antonini *et al.* (1999) noted that the Sr–Nd–Pb isotope signatures are consistent with the origin put forward by Hergt *et al.* (1989*b*), and they proposed that Ferrar magmas were generated by high degrees of partial melting of an enriched mantle (E-MORB type) which later interacted with crustal materials during assimilation–fractionation–crystallization processes. However, their contention that crustal-level interaction between mantle-derived magmas and lower continental crust (granulite) created the geochemical characteristics of their least-evolved Ferrar rock (MgO = 5.3%) has been questioned (Hergt 2000).

The geochemical characteristics of the olivine-bearing dolerites (MgO = 9%, together with low abundances of HFSEs, and crust-like trace element patterns and isotopes) compound the problem of the mantle origin. To help elucidate the mantle source, Molzahn *et al.* (1996) and Brauns *et al.* (2000) examined Os isotopes in Ferrar and Tasmanian tholeiites: the former consist of lavas and one sill sample, which has a high Mg# (71.9) but no petrographical evidence of olivine, whereas the latter consist of cumulates. The authors concluded that the mantle-like Os initial isotope ratios of whole rocks and minerals (Ferrar) and oxides (Tasmania) require assimilation of crustal materials prior to the generation of Ferrar magmas in the mantle. Hergt and Brauns (2001) evaluated the constraints on possible source compositions, whether it was a depleted subcontinental lithospheric mantle or a plume-related mantle modified by an enriched partial melt, and concluded that it was still unresolved. Alternatively, Mukasa *et al.* (2003) suggested a previously melted harzburgitic mantle later enriched by subduction processes as the Ferrar source. Subsequently, Mukasa *et al.* (2007) argued that the PGE abundances (extreme depletion in Os and Ir compared to Ru, Pt and Pd) are incompatible with a plume origin and proposed that the FLIP magmas originated by decompression melting in a subduction zone. Foden *et al.* (2012) advocated, on the basis of major elements, for the Ferrar magmas being derived from a mantle source more depleted than MORB. To account for the lithophile trace elements and isotopic compositions, they suggested melting of a depleted harzburgitic lithospheric source contaminated by a small fraction of upper crustal material.

With emphasis on the high SiO_2 of the Ferrar rocks, a model involving hydrous and anhydrous melting of fertile and depleted spinel lherzolites has been proposed by Demarchi *et al.* (2001). However, this model was put forward without consideration of isotope data. Further alternatives were proposed by Ivanov *et al.* (2017), who invoked either wet-sediment subduction and slab dehydration at the mantle transition or mantle melting followed by metasomatism involving subduction-derived fluids as mechanisms for generating the Ferrar geochemical characteristics.

Whatever the source, it had to have been enriched isotopically relative to E-MORB, and have HFSE element depletions greater than, and REE abundances lower than, E-MORB, yet carrying a crustal signature. Sediment subduction into the mantle appears to be mandated in order to generate the 'crustal' signature. Using PGE abundances and Os isotopic data, Choi *et al.* (2019*a*) argued that the Ferrar signature was acquired as a result of wet-sediment subduction and metasomatism of the overlying mantle wedge. The mantle wedge, converted to a hydrated peridotite–pyroxenite mix, underwent decompression melting in an extensional regime. This tectonic regime, initiated earlier in the Jurassic (Elliot *et al.* 2016), controlled the decompression and facilitated the rapid generation of magma, which led to the short duration of emplacement. Choi *et al.* (2019*b*) further suggested that decompression melting was a far-field effect of plume-related instabilities in the proto-Weddell Sea region.

Transport path

The linear distribution and geochemical coherence of Ferrar magmatic rocks has raised significant questions regarding the geographical location of their mantle source. Two alternatives have been presented: were the Ferrar magmas generated at a number of centres along the linear outcrop pattern, or were they generated at a point source and migrated laterally at depths, in some cases for thousands of kilometres?

Elliot (1976) and Cox (1978) advocated, and Storey and Alabaster (1991) similarly suggested, a line source for the Ferrar province magmas, in which magmas were generated from domains in the mantle directly underlying the region of magma emplacement and with minimal lateral transport. Given the linear geographical extent of the province, it was related to the Gondwana plate margin, which had been active for much of the Paleozoic Era and into Mesozoic (early Jurassic) time. The notion of a line source is not inconsistent with the models that require generation of an enriched lithospheric mantle source resulting from the incorporation of subducted sediment.

The linear model involves magma generation along a trend parallel or sub-parallel to the Antarctic basement boundary. That boundary delineates a substantial crustal thickness change (*c.* >35 km thick craton v. *c.* <25 km in West Antarctica: Chaput *et al.* 2014; Ramirez *et al.* 2017), and thus might have controlled the sites of Ferrar magma generation. Over a distance of 3500 km, the linear trend crosses several lithospheric provinces (Fig. 18) and magmas with a variety of geochemical and isotopic characteristics might be expected due to variations in source composition and extents of partial melting, in contrast to the geochemical coherence of the Ferrar magmas. A key might be the trend of the crustal thickness change, a fundamental property of the Antarctic Plate in that it marks the boundary between basement terrains and Phanerozoic orogenic belts (Elliot 2013). In this scenario, magma generation would be controlled by the trend of the early Paleozoic Ross Orogen. To generate the geochemically coherent Ferrar rocks spread over 3500 km there would have to have

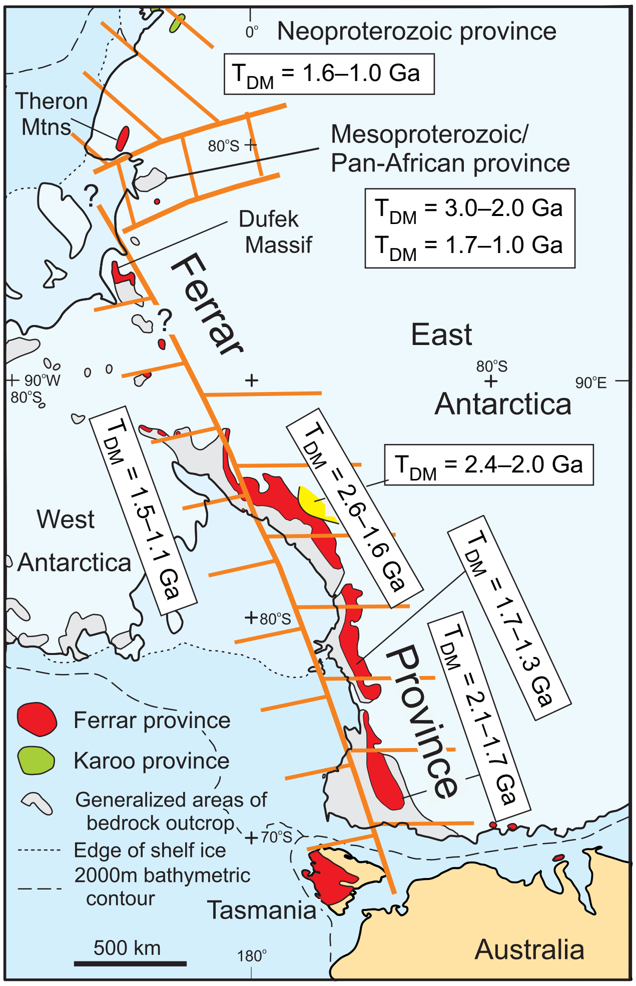

Fig. 18. Distribution of the Ferrar Large Igneous Province and lithospheric domains. The approximate domain margins are marked by solid orange lines and the inferred extent of the domains by orange 'ladders'. The Precambrian domain bordering the central Transantarctic Mountains is in yellow. Data sources for domains: Armienti *et al.* (1990), Borg *et al.* (1990), Cox *et al.* (2000), Leat *et al.* (2005), Black *et al.* (2010), Will *et al.* (2010), Loewy *et al.* (2011) and Goodge *et al.* (2012). The original lateral extent of the Ferrar province is largely speculative. T_{DM}, depleted mantle model age.

been a uniform mantle source reservoir modified by the incorporation of a consistent amount of subducted sediment of uniform composition, and uniformity in the composition of magmas generated. The creation of such a widespread uniform reservoir by subduction-related processes seems most unlikely.

An alternative (and preferred) hypothesis, a geographically restricted source combined with large-scale lateral transport, was first proposed by Fleming *et al.* (1997) because of the geochemical coherence of the Ferrar magmas, and by Storey and Kyle (1997), but the transport paths differed (see Elliot and Fleming 2017). The unique chemistry and tightly constrained composition of the SPCT led Elliot *et al.* (1999) to advocate long-distance transport of Ferrar magmas and suggested migration at various crustal depths. Strong support for a single source is given by the fact that, in the linear model, magmas from subjacent mantle sources would have traversed several different lithospheric provinces, as first noted by Leat (2008) (Fig. 18). However, this is not reflected in the coherent isotope characteristics of the Ferrar rocks and, in particular, the evolved but highly restricted SPCT composition, which would require identical magma generation and evolutionary processes, and identical end products over a linear distance of more than 3000 km. In this model, Ferrar magmas were generated in the lithospheric mantle, migrated into the crust and were then dispersed laterally at mid- to lower-crustal depths. The possibility of such long-distance transport is demonstrated by the Mackenzie dyke swarm (Baragar *et al.* 1996; Ernst and Buchan 1997), which was emplaced at mid-crustal depths and has been traced for 2500 km across the Canadian Shield.

Storey and Kyle (1997) argued for supracrustal transport through sills, and Ferris *et al.* (2003) further suggested that the Dufek intrusion formed the crustal magma chamber from which the Ferrar magmas migrated along the Transantarctic Mountains. Airoldi *et al.* (2016) and Magee *et al.* (2016) also advocated long-distance transport through sills. The contention that Mg# and MgO decrease from the point of origin along the length of the Transantarctic Mountains (Leat 2008; Magee *et al.* 2016, 2019) is misleading because, for the province as a whole, it is not supported by the geochemical data for the lavas nor for the sills. There is no spatial pattern with respect to the inferred proto-Weddell Sea source region (Elliot and Fleming 2017) (Fig. 7). In addition, long-distance sill transport throughout the province is regarded as improbable because it requires magmas to cross a pre-Devonian palaeotopographical high separating the central Transantarctic Mountains from south Victoria Land (the Ross High of Collinson *et al.* 1994), and another palaeotopographical high separating the south and north Victoria Land Beacon basins (Collinson *et al.* 1994) (Fig. 19). Magmas would also have to be transported to the Permo-Triassic basin of Tasmania (Veevers *et al.* 1994), the relationship of which to the north Victoria Land basin is uncertain because it is offset from, not along strike with, the north Victoria Land basin in a Gondwana reconstruction. In south Victoria Land, magmas would have had to burrow down hundreds of metres through the Taylor Group and penetrate basement granitic and gneissic rocks in the Dry Valleys region to form the very thick Basement Sill and its associated feeder (Fig. 20). That proposed feeder, on rising from depth, must have traversed basement rock. In addition, there are examples of dykes cutting the pre-Devonian basement in the Dry Valleys region and elsewhere in south Victoria Land (Darwin Glacier and Prince Albert Mountains regions: Haskell *et al.* 1965; Skinner and Ricker 1968, respectively). Dolerite intrusions, including thick sills, are also present in basement granitic rocks at the Nilsen Plateau (McLelland 1967), Mount Weaver (Doumani and Minshew 1965) and at Thanksgiving Point alongside the Shackleton Glacier (Figs 1 & 5). Thick dykes transecting basement rocks are few and widely scattered, but indicate transport of magmas from depth at those sites (Elliot and Fleming 2004), not transport through supracrustal sills. Dykes have been inferred geophysically to extend southwards from the Dufek intrusion (Ferris *et al.* 2003) and to occur at depth orientated parallel to major structures in the central Transantarctic Mountains (Goodge and Finn 2010); however, no major dyke swarms, such as occur in the Karoo of southern Africa (e.g. Coetzee and Kisters 2018), have been identified. Some support for transport in the lower crust is given by Ramirez *et al.* (2017), who suggested that geophysically interpreted mafic layering within or near the base of the crust of the Transantarctic Mountains may be related to the FLIP.

The actual path taken by the magmas at depth remains speculative (Fig. 21). In the Ross Sea sector of the Transantarctic Mountains, the outcrop distribution, the occurrence of dykes and the proposed Basement Sill feeder, and the phreatomagmatic centres all suggest that magmas migrated locally into supracrustal rocks to form sills and to the surface to be erupted as lavas and pyroclastic rocks. Although Karoo dolerite sills were not intruded into Cape Fold Belt deformed strata, the Dufek intrusion in the Weddell Sea sector was

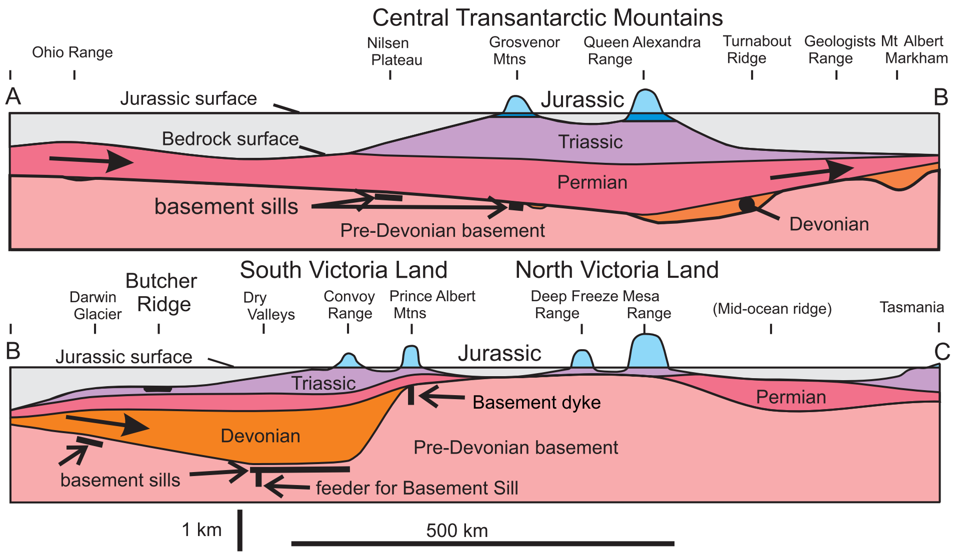

Fig. 19. Diagrammatic section from the Ohio Range to Tasmania (see Fig. 1) along the length of the Transantarctic Mountains to illustrate the current distribution of extrusive rocks, and the known distribution of sills and dykes cutting basement rocks (projected onto the line of section). Sills are present in all stratigraphic successions. Permian strata thin markedly, or are absent, over palaeogeographical highs. Heavy arrows denote magma paths if transport from the point of origin were through supracrustal sills.

emplaced by vertical magma migration into the folded Paleozoic strata of the Pensacola Mountains, the only such instance in the Ferrar province. The Ferrar extrusive rocks in the Ross Sea sector are interpreted to have been erupted into a rift valley system (Elliot and Fleming 2008), which is now located on the edge of the pre-Devonian basement and close to the lithospheric boundary between cratonic East Antarctica and the outboard Paleozoic orogenic belts that form the disrupted and displaced continental fragments making up West Antarctica (Dalziel and Lawver 2001). The geophysical interpretation of Ferrar rocks occupying a rift or rifts in the Wilkes Subglacial Basin in the hinterland of north Victoria Land (Ferraccioli *et al.* 2009) suggests other rift basins in the hinterland of the Transantarctic Mountains might have existed in Jurassic time.

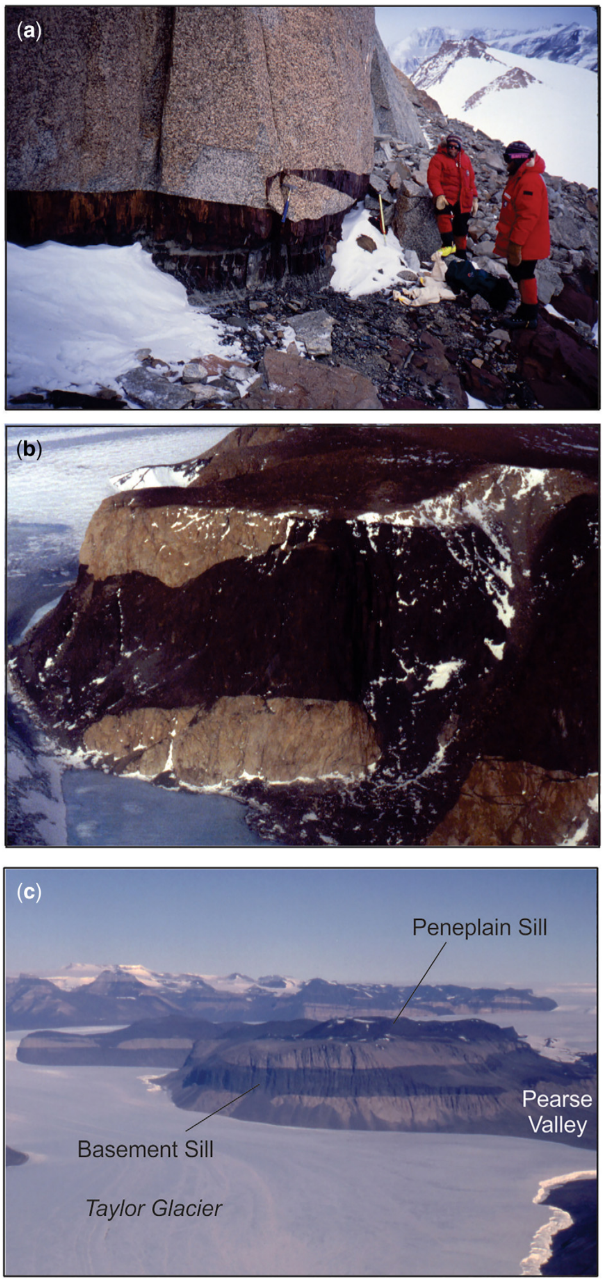

Fig. 20. Olivine-bearing dolerite sills emplaced in pre-Devonian basement rocks. (**a**) A sill cutting basement granite at the Nilsen Plateau, central Transantarctic Mountains (Fig. 1). (**b**) A sill at Thanksgiving Point, central Transantarctic Mountains. View to the NW (Fig. 5). (**c**) The Basement Sill intruding Cambro-Ordovician granitoid near Pearse Valley, south Victoria Land (Fig. 6). The Peneplain Sill was intruded along or close to the non-conformity separating basement rock from Devonian strata. View to the SE. (Images: T.H. Fleming.)

Some outstanding issues

The generation of the mantle source composition: the most basic Ferrar magmas (MgO = 9–10%) have high SiO_2 (52%), enriched Sr and Nd isotope compositions, mantle oxygen and Os isotope compositions, and trace elements with low abundances but crustal patterns. These characteristics imply an unusual mantle source that is subduction-related rather than plume-related. What new studies might verify the proposal that partial melting of peridotitic material, metasomatized by subducted sediment, in the mantle wedge below the Gondwana margin generated Ferrar primary magmas?

If Ferrar magmas are subduction-related and have distributed sources along its outcrop length, why does the Ferrar province exhibit such geochemical coherence? Why is there so little magma diversity beyond the single MFCT trend and the restricted SPCT composition? In particular, what controlled the generation of the SPCT composition, which is identical for over 3000 km?

Assuming it is not simple vertical migration of magma from the mantle along the length of the Ferrar province, what is the transport path for crustal dispersal from the putative proto-Weddell Sea point source? Why do the Ferrar magmas show no spatial pattern of changing composition related to distance from the source?

What are the flow patterns in sills in the various regions? Would they show dispersion from central conduits, as is the case for the Basement Sill in the Dry Valleys region?

Would careful evaluation of sill geometry reveal saucer-shaped intrusions, such as are documented in the Karoo?

Can age determinations clarify if emplacement of the Ferrar magmas differs in timing along the length of the Transantarctic Mountains? Is there a determinable age difference between the olivine-bearing dolerite sills and the rest of the MFCT, and between the MFCT and SPCT tholeiites?

How far does the Ferrar Province extend subglacially under the East Antarctic Ice Sheet and into the Ross Embayment?

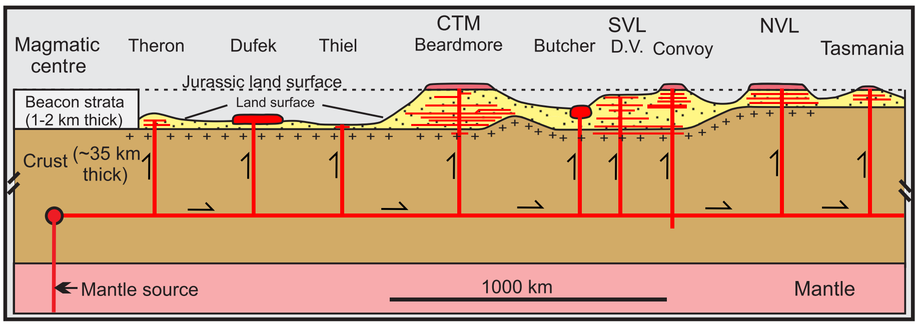

Fig. 21. Schematic model for a Ferrar magma transport path in the crust from an inferred mantle source in the proto-Weddell Sea region to Tasmania. A possible site where magmas are inferred to have started migrating laterally is represented by the circle, which is located at mid- to lower-crustal depths. The ultimate magma source resided in the mantle below the proto-Weddell Sea region. D.V., Dry Valleys; CTM, central Transantarctic Mountains; NVL, north Victoria Land; SVL, south Victoria Land.

Is the Dufek intrusion definitively one or two bodies?

Can a chilled margin composition be identified and/or liquid compositions be reconstructed for the Dufek intrusion?

Is there any clue to the lower hidden section of the Dufek intrusion in the sediments derived from it in the Filchner Trough region?

Are any of the inferred basaltic bodies in the Weddell Sea sector, such as Berkner Island and the dipping reflector sequences offshore Coats Land (Hunter *et al.* 1996; Jordan *et al.* 2017), part of the FLIP?

Do Ferrar compositions occur for certain in the Karoo Large Igneous Province? If so, are they confined to the region south and east of Lesotho?

Summary

The Ferrar Large Igneous Province (FLIP) differs from all other such provinces in that it has an extant linear outcrop pattern and its emplacement was probably controlled by lithospheric structure, which itself is defined by the boundary between the craton and Phanerozoic belts, and by the early Jurassic extensional tectonic regime. Geochemically, the province is unique among large igneous provinces (LIPs) in significant Sr, Nd and Pb isotope enrichment, and the low abundances of high field strength elements (HFSEs) and their crustal pattern even in the most basic olivine-bearing dolerites. The coherence of the province-wide geochemical data for the Mount Fazio Chemical Type (MFCT) compositions suggests a common origin in the mantle and similar evolutionary processes. Both models for the source – the single source and long-distance transport model, and the linear source model with multiple sites of mantle origin – have uncertainties. The highly evolved Scarab Peak Chemical Type (SPCT) composition strongly implies a single source region and evolution, and long-distance magma transport. The processes in the mantle source region that resulted in the Ferrar magmas, most probably involving assimilation of subducted material and then melting to produce the primary magma composition, remain somewhat uncertain.

Acknowledgements Reviews by Janet Hergt and Marco Brenna are much appreciated and have considerably improved the manuscript. In particular, the authors thank John Smellie for the invitation to contribute to this Memoir. This is Byrd Polar and Climate Research Center contribution No. 1581.

Author contributions **DHE**: data curation (supporting), formal analysis (equal), investigation (equal), writing – original draft (lead), writing – review & editing (equal); **THF**: data curation (lead), formal analysis (equal), investigation (equal), writing – original draft (supporting), writing – review & editing (equal).

Funding The authors acknowledge significant support over many years from the Office of Polar Programs, National Science Foundation, Washington, DC.

Data availability All data are either already published, included in the tables in this paper, or in the case of unpublished data, can be obtained, upon reasonable request, from the authors

Appendix A: Grid references for field photographs and samples in Tables 3 and 5

Location	Longitude	Latitude
Figure 2a: Point 3120, Nilsen Plateau	159° 15.5′ W	86° 28.4′ S
Figure 2b: Mount Joyce	160° 49′ E	75° 36′ S
Figure 3a: East of Mount Gran	161° 06.0′ E	76° 58.5′ S
Figure 3b: Terra Cotta Mountain	161° 15′ E	77° 54′ S
Figure 4a: Shenk Peak	174° 45′ W	85° 11′ S
Figure 4b: Dismal Buttress	178° 00′ W	85° 27′ S
Figure 8a: Rougier Hill, lowest sill	174° 33.4′ W	85° 09.5′ S
Figure 8b: Rougier Hill, lowest sill	174° 33.4′ W	85° 09.5′ S
Figure 18a: Cougar Cyn, Nilsen Plateau	160° 40.0′ W	86° 18.4′ S
Figure 18b: Thanksgiving Point	177° 00.0′ W	84° 56.7′ S
Figure 18c: SE of Pearse Valley	161° 34.7′ E	77° 45.0′ S
Sill near Dawson Peak	162° 25.2′ E	83° 50.5′ S
Lavas at Storm Peak (Peterson Ridge)	163° 55.7′ E	84° 34.1′ S
Sill near Mount Achernar	160° 53.9′ E	84° 11.3′ S

Coordinates without a decimal point from are the Gazetteer of Antarctic.
Place names with a decimal point are from USGS topographical sheets.

References

Airoldi, G.M., Muirhead, J.D., Long, S.M., Zanella, E. and White, J.D.L. 2016. Flow dynamics in mid-Jurassic dikes and sills of the Ferrar large igneous province and implications for long-distance transport. *Tectonophysics*, **682**, 182–199, https://doi.org/10.1016/j.tecto.2016.06.029

Allibone, A.H., Forsyth, P.J., Sewell, R.J., Turnbull, I.M. and Bradshaw, M.A. 1991. *Geology of the Thundergut Area, Southern Victoria Land, Antarctica, Scale 1:50 000*. New Zealand Geological Survey Miscellaneous Geological Map, **21**.

Antonini, P., Demarchi, G., Piccirillo, E.M. and Orsi, G. 1997. Distinct magma pulses in the Ferrar tholeiites of Thern Promontory (Victoria Land, Antarctica). *Terra Antartica*, **4**, 33–39.

Antonini, P., Piccirillo, E.M., Petrini, R., Civetta, L., D'Antonio, M. and Orsi, G. 1999. Enriched mantle – Dupal signature in the genesis of the Jurassic Ferrar tholeiites from Prince Albert Mountains (Victoria Land, Antarctica). *Contributions to Mineralogy and Petrology*, **136**, 1–19, https://doi.org/10.1007/s004100050520

Armienti, P., Ghezzo, C., Innocenti, F., Manetti, P., Rocchi, S. and Tonarini, S. 1990. Isotope geochemistry and petrology of granitoid suites from Granite Harbour Intrusives of the Wilson Terrane, north Victoria Land, Antarctica. *European Journal of Mineralogy*, **2**, 103–123, https://doi.org/10.1127/ejm/2/1/0103

Baragar, W.R.A., Ernst, R.E., Hulbert, L. and Peterson, T. 1996. Longitudinal petrochemical variation in the Mackenzie Dyke Swarm, northwestern Canadian Shield. *Journal of Petrology*, **37**, 317–359, https://doi.org/10.1093/petrology/37.2.317

Barrett, P.J. 1991. The Devonian to Triassic Beacon Supergroup of the Transantarctic Mountains and correlatives in other parts of Antarctica. *Oxford Monographs on Geology and Geophysics*, **17**, 120–152.

Barrett, P.J., Elliot, D.H. and Lindsay, J.F. 1986. The Beacon Supergroup (Devonian–Triassic) and Ferrar Group (Jurassic) in the Beardmore Glacier area, Antarctica. *Antarctic Research Series*, **36**. American Geophysical Union, Washington, DC, 339–428.

Bédard, J.J., Marsh, B.D., Hersum, T.G., Naslund, H.R. and Mukasa, S.B. 2007. Large-scale mechanical redistribution of orthopyroxene and plagioclase in the Basement Sill, Ferrar Dolerites, McMurdo Dry Valleys, Antarctica: Petrological, mineral–chemical and field evidence for channelized movement of crystals and melt. *Journal of Petrology*, **48**, 2289–2326, https://doi.org/10.1093/petrology/egm060

Behrendt, J.C., Drewry, D.J., Jankowski, E. and Grim, M.S. 1981. Aeromagnetic and radio echo ice-sounding measurements over the Dufek intrusion, Antarctica. *Journal of Geophysical Research*, **86**, 3014–3020, https://doi.org/10.1029/JB086iB04p03014

Behrendt, J.C., Damaske, D., Finn, C.A., Kyle, P.R. and Wilson, T.J. 2002. Draped aeromagnetic survey in Transantarctic Mountains over area of Butcher Ridge igneous complex showing extent of underlying mafic intrusion. *Journal of Geophysical Research: Solid Earth*, **107**, EPM 3-1–EPM 3-10, https://doi.org/10.1029/2001JB000376

Benson, W.N. 1916. Report on the Petrology of the Dolerites collected by the British Antarctic Expedition, 1907–09. *Reports of Scientific Investigations, Geology*, **II**, 153–160.

Black, L.P., Everard, J.L. *et al*. and 2010. Controls on Devonian–Carboniferous magmatism in Tasmania, based on inherited zircon age patterns, Sr, Nd and Pb isotopes, and major and trace element geochemistry. *Australian Journal of Earth Sciences*, **57**, 933–968, https://doi.org/10.1080/08120099.2010.509407

Borg, S.G., DePaolo, D.J. and Smith, B.M. 1990. Isotopic structure and tectonics of the central Transantarctic Mountains. *Journal of Geophysical Research*, **95**, 6647–6667.

Boudreau, A. and Simon, A. 2007. Crystallization and degassing in the Basement Sill, McMurdo Dry Valleys, Antarctica. *Journal of Petrology*, **48**, 1369–1386, https://doi.org/10.1093/petrology/egm022

Bradshaw, M.A. 2013. The Taylor Group (Beacon Supergroup): the Devonian sediments of Antarctica. *Geological Society, London, Special Publications*, **381**, 67–97, https://doi.org/10.1144/SP381.23

Brauns, C.M., Hergt, J.M., Woodhead, J.D. and Maas, R. 2000. Os isotopes and the origin of the Tasmanian Dolerites. *Journal of Petrology*, **41**, 905–918, https://doi.org/10.1093/petrology/41.7.905

Brewer, T.S., Hergt, J.M., Hawkesworth, C.J., Rex, D. and Storey, B.C. 1992. Coats Land dolerites and the generation of Antarctic continental flood basalts. *Geological Society, London, Special Publications*, **68**, 185–208, https://doi.org/10.1144/GSL.SP.1992.068.01.12

Bromfield, K., Burrett, C.F., Leslie, R.A. and Meffre, S. 2007. Jurassic volcaniclastic–basaltic andesite–dolerite sequence in Tasmania: new age constraints for fossil plants from Lune River. *Australian Journal of Earth Sciences*, **54**, 965–974, https://doi.org/10.1080/08120090701488297

Brotzu, P., Capaldi, G., Civetta, L., Melluso, L. and Orsi, G. 1988. Jurassic Ferrar dolerites and Kirkpatrick basalts in northern Victoria Land (Antarctica): stratigraphy, geochronology and petrology. *Memorie della Societa Geologica Italiana*, **43**, 97–116.

Brotzu, P., Capaldi, G., Civetta, L., Orsi, G., Gallo, G. and Melluso, L. 1992. Geochronology and geochemistry of Ferrar rocks from north Victoria Land, Antarctica. *European Journal of Mineralogy*, **4**, 605–617, https://doi.org/10.1127/ejm/4/3/0605

Browne, W.R. 1923. The dolerites of King George Land and Adelie Land. *Australasian Antarctic Expedition, 1911–14, Scientific Reports Series A, Geology*, **3**, 245–258.

Burgess, S.D., Bowring, S.A., Fleming, T.H. and Elliot, D.H. 2015. High precision geochronology links the Ferrar Large Igneous Province with early Jurassic ocean anoxia and biotic crisis. *Earth and Planetary Science Letters*, **415**, 90–99, https://doi.org/10.1016/j.epsl.2015.01.037

Carnes, J.D., Cheadle, M., Gee, J.S., Grimes, C.B. and Swapp, S.M. 2011. The magmatic and thermal history of the Dufek Complex, Antarctica. *Eos, Transactions of the American Geophysical Union*, Fall Meeting 2011, **92**, abstract V33C-2661.

Chaput, J., Aster, R.C. *et al*. 2014. The crustal thickness of West Antarctica. *Journal of Geophysical Research: Solid Earth*, **119**, 378–395, https://doi.org/10.1002/2013JB010642

Charrier, A.D. 2010. *Emplacement History of the Basement Sill, Antarctica: Injection Mechanics of Crystal-Laden Slurries*. PhD thesis, Johns Hopkins University, Baltimore, Maryland, USA.

Charrier, A.D. and Manochehri, S. 2013. The compaction of ultramafic cumulates in layered intrusions – time and length scales. *Eos, Transactions of the American Geophysical Union*, Fall Meeting 2013, **94**, abstract V54B-01.

Cheadle, M. and Gee, J.S. 2017. Quantitative textural insights into the formation of gabbro in mafic intrusions. *Elements*, **13**, 409–414, https://doi.org/10.2138/gselements.13.6.409

Cheadle, M., Meurer, W.P., Grimes, C.B., Gee, J.S. and McCullough, B.C. 2007. Understanding the magmatic construction of the Dufek complex, Antarctica. *Eos, Transactions of the American Geophysical Union*, **88**(52), Fall Meeting Supplement, abstract V53D-02.

Choi, S.H., Mukasa, S.B., Ravizza, G., Fleming, T.H., Marsh, B.D. and Bédard, J.H.J. 2019*a*. Fossil subduction zone origin for magmas in the Ferrar Large Igneous Province, Antarctica: Evidence from PGE and Os isotope systematics in the Basement Sill of the McMurdo Dry valleys. *Earth and Planetary Science Letters*, **506**, 507–519, https://doi.org/10.1016/j.epsl.2018.11.027

Choi, S.H., Mukasa, S.B., Ravizza, G., Fleming, T.H., Marsh, B.D. and Bédard, J.H.J. 2019*b*. Fossil subduction zone origin for magmas in the Ferrar Large Igneous Province, Antarctica: Evidence from PGE and Os isotope systematics in the Basement Sill of the McMurdo Dry valleys. *MantlePlumes.org*, http://www.mantleplumes.org/FerrarLIP.html

Coetzee, A. and Kisters, A.F.M. 2017. Dyke-sill relationships in Karoo dolerites as indicators of propagation and emplacement processes of mafic magmas in shallow crust. *Journal of Structural Geology*, **97**, 172–188, https://doi.org/10.1016/j.jsg.2017.03.002

Coetzee, A. and Kisters, A.F.M. 2018. The elusive feeders of the Karoo Large Igneous Province and their structural controls. *Tectonophysics*, **747–748**, 146–162, https://doi.org/10.1016/j.tecto.2018.09.007

Collinson, J.W., Elliot, D.H., Isbell, J.L. and Miller, J.M.G. 1994. Permian–Triassic Transantarctic Basin. *Geological Society of America Memoirs*, **184**, 173–222.

Compston, W., McDougall, I. and Heier, K.S. 1968. Geochemical comparison of rthe Mesozoic basaltic rocks of Antarctica, South Africa, South America and Tasmania. *Geochimica et Cosmochimica Acta*, **33**, 129–149, https://doi.org/10.1016/S0016-7037(68)80001-8

Cox, K.G. 1978. Flood basalts, subduction, and the break-up of Gondwanaland. *Nature*, **274**, 47–49, https://doi.org/10.1038/274047a0

Cox, S.C., Parkinson, D.L., Allibone, A.H. and Cooper, A.F. 2000. Isotopic character of Cambro-Ordovician plutonism, southern Victoria Land, Antarctica. *New Zealand Journal of Geology and Geophysics*, **43**, 501–520, https://doi.org/10.1080/00288306.2000.9514906

Dalziel, I.W.D. and Lawver, L.A. 2001. The lithospheric setting of the West Antarctic Ice Sheet. *American Geophysical Union Antarctic Research Series*, **77**, 29–44.

Delisle, G. and Fromm, K. 1989. Further evidence for a Cretaceous thermal event in north Victoria Land. *Geologisches Jahrbuch*, **38E**, 143–151.

Demarchi, G., Antonini, P., Piccirillo, E.M., Orsi, G., Civetta, L. and D'Antonio, M. 2001. Significance of orthopyroxene and major element constraints on the petrogenesis of Ferrar tholeiites from southern Prince Albert Mountains, Victoria land, Antarctica. *Contributions to Mineralogy and Petrology*, **142**, 127–146, https://doi.org/10.1007/s004100100287

Doumani, G.A. and Minshew, V.H. 1965. General geology of the Mount Weaver area, Queen Maud Mountains, Antarctica. *American Geophysical Union Antarctic Research Series*, **6**, 127–139.

Elliot, D.H. 1970. Jurassic tholeiites of the central Transantarctic Mountains, Antarctica. *In*: Gilmour, E.H. and Stradling, D. (eds) *Proceedings of the Second Columbia River Basalt Symposium, March 1969*. Eastern Washington State College Press, Cheney, WA, 301–325.

Elliot, D.H. 1976. Tectonic setting of the Jurassic Ferrar Group, Antarctica. *In*: Gonzalez, F.O. (ed.) *Proceedings of the Symposium* *on Andean and Antarctic Volcanology Problems*. IAVCEI Special Series, 357–372.

Elliot, D.H. 2013. The geological and tectonic evolution of the Transantarctic Mountains: a review. *Geological Society, London, Special Publications*, **381**, 7–35, https://doi.org/10.1144/SP381.14

Elliot, D.H. and Fleming, T.H. 2000. Weddell triple junction: The principal focus of Ferrar and Karoo magmatism during initial breakup of Gondwana. *Geology*, **28**, 539–542, https://doi.org/10.1130/0091-7613(2000)28<539:WTJTPF>2.0.CO;2

Elliot, D.H. and Fleming, T.H. 2004. Occurrence and dispersal of magmas in the Jurassic Ferrar Large Igneous Province, Antarctica. *Gondwana Research*, **7**, 223–237, https://doi.org/10.1016/S1342-937X(05)70322-1

Elliot, D.H. and Fleming, T.H. 2008. Physical volcanology and geological relationships of the Ferrar Large Igneous Province, Antarctica. *Journal of Volcanology and Geothermal Research*, **172**, 20–37, https://doi.org/10.1016/j.jvolgeores.2006.02.016

Elliot, D.H. and Fleming, T.H. 2017. The Ferrar large Igneous Province: field and geochemical constraints on supra-crustal (high-level) emplacement of the magmatic system. *Geological Society, London, Special Publications*, **463**, 41–58, https://doi.org/10.1144/SP463.1

Elliot, D.H., Fleming, T.H., Haban, M.A. and Siders, M.A. 1995. Petrology and mineralogy of the Kirkpatrick Basalt and Ferrar Dolerite, Mesa Range region, north Victoria Land, Antarctica. *American Geophysical Union Antarctic Research Series*, **67**, 103–141.

Elliot, D.H., Fleming, T.H., Kyle, P.R. and Foland, K.A. 1999. Long Distance Transport of Magmas in the Jurassic Ferrar Large Igneous Province, Antarctica. *Earth and Planetary Science Letters*, **167**, 87–104, https://doi.org/10.1016/S0012-821X(99)00023-0

Elliot, D.H., Larsen, D., Fanning, C.M., Fleming, T.H. and Vervoort, J.D. 2016. The Lower Jurassic Hanson Formation of the Transantarctic Mountains: implications for the Antarctic sector of the Gondwana Plate margin. *Geological Magazine*, **154**, 777–803, https://doi.org/10.1017/S0016756816000388

Elliot, D.H., White, J.D.L. and Fleming, T.H. 2021. Ferrar Large Igneous Province: volcanology. *Geological Society, London, Memoirs*, **55**, https://doi.org/10.1144/M55-2018-44

Ernst, R.E. and Buchan, K.L. 1997. Giant radiating dyke swarms: their use in identifying Pre-Mesozoic large igneous provinces and mantle plumes. *American Geophysical Union Geophysical Monograph Series*, **100**, 247–272.

Faure, G. and Mensing, T.M. 1993. K–Ar dates and paleomagnetic evidence for Cretaceous alteration of Mesozoic basaltic lava flows, Mesa Range, northern Victoria Land, Antarctica. *Chemical Geology*, **109**, 305–315, https://doi.org/10.1016/0009-2541(93)90077-V

Faure, G., Hill, R.L., Jones, L.M. and Elliot, D.H. 1972. Isotope composition of strontium and silica content of Mesozoic basalt and dolerite from Antarctica. *In*: Adie, R.J. (ed.) *Antarctic Geology and Geophysics*. Universitetsforlaget, Oslo, 617–624.

Faure, G., Bowman, J.R., Elliot, D.H. and Jones, L.M. 1974. Strontium isotope composition and petrogenesis of the Kirkpatrick Basalt, Queen Alexandra Range, Antarctica. *Contributions to Mineralogy and Petrology*, **48**, 153–169, https://doi.org/10.1007/BF00383353

Faure, G., Pace, K.K. and Elliot, D.H. 1982. Systematic variations of $^{87}Sr/^{86}Sr$ ratios and major element concentrations in the Kirkpatrick Basalt of Mt. Falla, Queen Alexandra Range, Transantarctic Mountains. *In*: Craddock, C. (ed.) *Antarctic Geoscience*. University of Wisconsin Press, Madison, WI, 715–723.

Faure, G., Hoefs, J. and Mensing, T.M. 1984. Effect of oxygen fugacity on sulfur isotope compositions and magnetite concentrations in the Kirkpatrick Basalt, Mount Falla, Queen Alexandra Range, Antarctica. *Chemical Geology*, **46**, 301–311, https://doi.org/10.1016/0009-2541(84)90173-6

Faure, G., Mensing, T.M., Jones, L.M., Hoefs, J. and Kibler, E.M. 1991. Isotopic and geochemical studies of Ferrar Dolerite sills in the Transantarctic Mountains. *In*: Ulbrich, H. and Rocha Campos, A.C. (eds) *Gondwana Seven Proceedings. Papers presented at the Seventh International Gondwana Symposium, Sao Paulo, 1988*. Instituto Geosciências, Universidade de São Paulo, São Paulo, Brazil, 669–683.

Ferraccioli, F., Armadillo, E., Jordan, T., Bozzo, E. and Corr, H. 2009. Aeromagnetic exploration over the East Antarctic Ice Sheet: A new view of the Wilkes Subglacial Basin. *Tectonophysics*, **478**, 62–77, https://doi.org/10.1016/j.tecto.2009.03.013

Ferris, J.K., Johnson, A. and Storey, B.C. 1998. Form and extent of the Dufek intrusion, Antarctica, from newly compiled aeromagnetic data. *Earth and Planetary Science Letters*, **154**, 185–202, https://doi.org/10.1016/S0012-821X(97)00165-9

Ferris, J.K., Storey, B.C., Vaughan, A.P.M., Kyle, P.R. and Jones, P.C. 2003. The Dufek and Forrestal intrusions, Antarctica: A centre for Ferrar Large Igneous Province dike emplacement? *Geophysical Research Letters*, **30**, 1348, https://doi.org/10.1029/2002GL016719

Fitzgerald, P.G. 2002. Tectonics and landscape evolution of the Antarctic Plate since the breakup of Gondwana, with an emphasis on the West Antarctic rift system and the Transantarctic Mountains. *Bulletin of the Royal Society of New Zealand*, **35**, 453–469.

Fleming, T.H. 1995. *Isotopic and Chemical Evolution of the Ferrar Group, Beardmore Glacier Region, Antarctica*. PhD thesis, Ohio State University, Columbus, Ohio, USA.

Fleming, T.H., Elliot, D.H., Jones, L.M. and Bowman, J.R. 1989. Secondary alteration or iron-rich tholeiitic rocks of the Kirkpatrick Basalt, northern Victoria Land. *Antarctic Journal of the United States*, **24**, 37–40.

Fleming, T.H., Foland, K.A., Elliot, D.H. and Miller, C.A. 1998. Isotopic and chemical constraints on the magmatic evolution of the Kirkpatrick Basalt, Carapace Nunatak, south Victoria Land, Antarctica. *Geological Society of America, Abstracts with Programs*, **30**(2), 17.

Fleming, T.H., Elliot, D.H., Jones, L.M., Bowman, J.R. and Siders, M.A. 1992. Chemical and isotopic variations in an iron-rich lava flow from North Victoria Land, Antarctica: Implications for low-temperature alteration and the petrogenesis of Ferrar magmas. *Contributions to Mineralogy and Petrology*, **111**, 440–457, https://doi.org/10.1007/BF00320900

Fleming, T.H., Elliot, D.H., Foland, K.A., Jones, L.M. and Bowman, J.R. 1993. Disturbance of Rb–Sr and K–Ar isotopic systems in the Kirkpatrick Basalt, North Victoria Land, Antarctica: Implications for mid-Cretaceous tectonism. *In*: Findlay, R.H., Banks, M.R., Veevers, J.J. and Unrug, R. (eds) *Gondwana 8 – Assembly, Evolution, and Dispersal*. Balkema, Rotterdam, The Netherlands, 411–424.

Fleming, T.H., Foland, K.A. and Elliot, D.H. 1995. Isotopic and chemical constraints on the crustal evolution and source signature of Ferrar magmas, North Victoria Land, Antarctica. *Contributions to Mineralogy and Petrology*, **121**, 217–236, https://doi.org/10.1007/BF02688238

Fleming, T.H., Heimann, A., Foland, K.A. and Elliot, D.H. 1997. $^{40}Ar/^{39}Ar$ geochronology of Ferrar Dolerite sills from the Transantarctic Mountains, Antarctica: Implications for the age and origin of the Ferrar Magmatic Province. *Bulletin of the Geological Society of America*, **109**, 533–546, https://doi.org/10.1130/0016-7606(1997)109<0533:AAGOFD>2.3.CO;2

Fleming, T.H., Foland, K.A. and Elliot, D.H. 1999. Apophyllite $^{40}Ar/^{39}Ar$ and Rb-Sr geochronology: potential utility and application to the timing of secondary mineralization of the Kirkpatrick Basalt, Antarctica. *Journal of Geophysical Research: Solid Earth*, **104**, 20 081–20 095, https://doi.org/10.1029/1999JB900138

Fleming, T.H., Elliot, D.H. and Calhoun, A. 2005. Geographic variations in chilled margin chemistry of Jurassic dolerite intrusions in the Dry Valley region of south Victoria Land, Antarctica. *Eos, Transactions of the American Geophysical Union*, **86**(52), Fall Meeting Supplement, V14C–V102.

Fleming, T.H., Burgess, S.D., Elliot, D.H. and Bowring, S. 2012. Space–time–geochemical constraints on the emplacement of the Ferrar Large Igneous Province in South Victoria Land, Antarctica. *Geological Society of America Abstracts with Programs*, **44**(7), 541.

Foden, J., Sossi, P., Segui, D., Robinson, F. and Tappert, R. 2012. The implications of mantle lithospheric delamination for the termination of Cambrian Pacific margin orogenesis: the creation of the source of the Tasmanian–Ferrar Jurassic large igneous province. *In*: *34th International Geological Congress (IGC) Australia 2012, Brisbane Convention and Exhibition Centre (BCEC), Queensland, Australia, 5–10 August 2012: Congress Handbook*. Australian Geoscience Council, Canberra, abstract 3818.

Ford, A.B. 1976. *Stratigraphy of the Layered Gabbroic Dufek Intrusion*. United States Geological Survey Bulletin, **1405–D**.

Ford, A.B. and Boyd, W.W. 1968. The Dufek intrusion – a major stratiform gabbroic body in the Pensacola Mountains. *In*: *Proceedings of the 23rd International Geological Congress, Prague, August 1968, Volume 2*, Academia, Prague, 13–28.

Ford, A.B. and Himmelberg, G.R. 1991. Geology and crystallization of the Dufek intrusion. *Oxford Monographs on Geology and Geophysics*, **17**, 175–214.

Ford, A.B. and Kistler, R.W. 1980. K–Ar age, composition, and origin of Mesozoic mafic rocks related to Ferrar Group, Pensacola Mountains, Antarctica. *New Zealand Journal of Geology and Geophysics*, **23**, 371–390, https://doi.org/10.1080/00288306.1980.10424146

Ford, A.B., Kistler, R.W. and White, L.D. 1986. Strontium and oxygen isotope study of the Dufek Intrusion. *Antarctic Journal of the United States*, **21**, 63–66.

Forsha, C.J. and Zieg, M.J. 2007. Mineralogy and Texture of the Peneplain sill, McMurdo Dry Valleys, Antarctica. *Eos, Transactions of the American Geophysical Union*, **88**(52), Fall Meeting Supplement, abstract V43A-1121.

Galerne, C.Y., Neumann, E-R. and Planke, S. 2008. Emplacement mechanisms of sill complexes: Information from the geochemical architecture of the Golden Valley Sill complex, South Africa. *Journal of Volcanology and Geothermal Research*, **177**, 425–440, https://doi.org/10.1016/j.jvolgeores.2008.06.004

Galerne, C.Y., Galland, O., Neumann, E. and Planke, S. 2011. 3D relationships between sills and their feeders: evidence from the Golden Valley Sill Complex (Karoo Basin) and experimental modelling. *Journal of Volcanology and Geothermal Research*, **202**, 189–199, https://doi.org/10.1016/j.jvolgeores.2011.02.006

Gee, J.S., Cheadle, M.J., Meurer, W.P. and Grimes, C.B. 2013. How big is the Dufek Intrusion? Paleomagnetic constraints on the cooling history of the Dufek layered intrusion. *Eos, Transactions of the American Geophysical Union*, Fall Meeting 2013, **94**, abstract GP34A-05.

Goodge, J.W. and Finn, C.A. 2010. Glimpses of East Antarctica: Aeromagnetic and satellite magnetic view from the central Transantarctic Mountains of West Antarctica. *Journal of Geophysical Research: Solid Earth*, **115**, https://doi.org/10.1029/2009JB006890

Goodge, J.W., Fanning, C.M., Norman, M.D. and Bennett, V.C. 2012. Temporal, isotopic and spatial relations of Early Paleozoic Gondwana-margin arc magmatism, central Transantarctic Mountains, Antarctica. *Journal of Petrology*, **53**, 2027–2065, https://doi.org/10.1093/petrology/egs043

Grapes, R.H. and Reid, D.L. 1971. Rythmic layering and multiple intrusion in the Ferrar Dolerite of South Victoria Land, Antarctica. *New Zealand Journal of Geology and Geophysics*, **14**, 600–604, https://doi.org/10.1080/00288306.1971.10421950

Grimes, C.B., Cheadle, M., Gee, J.S., Meurer, W.P., Swapp, S. and Lusk, M.W. 2008. The role of magma replenishment in the construction of the lower 500 m of the layered mafic Dufek intrusion. *Eos, Transactions of the American Geophysical Union*, **89**(53), Fall Meeting Supplement, abstract V13C-2134.

Gunn, B.M. 1962. Differentiation in Ferrar Dolerites, Antarctica. *New Zealand Journal of Geology and Geophysics*, **5**, 820–863, https://doi.org/10.1080/00288306.1962.10417641

Gunn, B.M. 1963. Layered intrusions in the Ferrar dolerites. *Mineralogical Society of America, Special Papers*, **1**, 124–133.

Gunn, B.M. 1966. Modal and element variation in Antarctic tholeiites. *Geochimica et Cosmochimica Acta*, **30**, 881–920, https://doi.org/10.1016/0016-7037(66)90026-3

Gunn, B.M. and Warren, G. 1962. *Geology of Victoria Land between the Mawson and Mulock Glaciers, Antarctica*. Bulletin of the Geological Survey of New Zealand, **71**.

Hamilton, W.B. 1964. Diabase sheets differentiated by liquid fractionation, Taylor Glacier region, south Victoria Land. *In*: Adie, R.J. (ed.) *Antarctic Geology*. North-Holland, Amsterdam, 442–454.

Hamilton, W.B. 1965. *Diabase Sheets of the Taylor Glacier Region, Victoria Land, Antarctica*. United States Geological Survey Professional Papers, **456-B**.

Hanemann, R. and Viereck-Götte, L. 2004. Geochemistry of Jurassic Ferrar lava flows, sills and dikes sampled during the joint German–Italian Antarctic Expedition 1999–2000. *Terra Antartica*, **11**, 39–54.

Hanemann, R. and Viereck-Götte, L. 2007*a*. Platinum-group elements in sills of the Jurassic Ferrar Large Igneous Province from northern Victoria Land, Antarctica. *United States Geological Survey Open-File Report*, **2007-1047**, Short Research Paper 032, https://doi.org/10.3133/ofr20071047srp032

Hanemann, R. and Viereck-Götte, L. 2007*b*. Evolution of low-Ti and high-Ti rocks of the Jurassic Ferrar Igneous Province, Antarctica: Constraints from crystallization experiments. *United States Geological Survey Open-File Report*, **2007-1047**, extended abstract 070.

Hanemann, R., Melcher, F., Mukasa, S.B., Viereck-Goette, L. and Abratis, M. 2009. PGE-enrichment with late-stage Fe–Ti oxide crystallization observed in the Dufek–Forrestal layered mafic intrusion, Antarctica. *Eos Transactions of the American Geophysical Union*, **90**(52), Fall Meeting Supplement, abstract V21A-1973.

Harris, M. 2014. *Geochemistry of some Ferrar Large Igneous Province Intrusive Rocks in the Transantarctic Mountains, Antarctica*. BS thesis, Ohio State University, Columbus, Ohio, USA.

Haskell, T.R., Kennett, J.P. and Prebble, W.M. 1965. Geology of the Brown Hills and Darwin Mountains, Antarctica. *Transactions of the Royal Society of New Zealand*, **2**, 231–248.

Heier, K.S., Compston, W. and McDougall, I. 1965. Thorium and uranium concentrations, and the isotope composition of strontium in the differentiated Tasmanian dolerites. *Geochimica et Cosmochimica Acta*, **29**, 643–659, https://doi.org/10.1016/0016-7037(65)90061-X

Heinonen, J.S., Carlson, R.W., Riley, T.R., Luttinen, A.V. and Horan, M.F. 2014. Subduction modified oceanic crust mixed with a depleted mantle reservoir in the sources of the Karoo continental flood basalt province. *Earth and Planetary Science Letters*, **394**, 229–241, https://doi.org/10.1016/j.epsl.2014.03.012

Hergt, J.M. 2000. Comment on: 'Enriched mantle – Dupal signature in the genesis of the Jurassic Ferrar tholeiites from Prince Albert Mountains (Victoria Land, Antarctica)' by Antonini P *et al.* (Contributions to Mineralogy and Petrology 136, 1–19; 1999). *Contributions to Mineralogy and Petrology*, **139**, 240–244, https://doi.org/10.1007/s004100000130

Hergt, J.M. and Brauns, C.M. 2001. On the origin of the Tasmanian dolerites. *Australian Journal of Earth Sciences*, **48**, 543–549, https://doi.org/10.1046/j.1440-0952.2001.00875.x

Hergt, J.M., Chappell, B.W., Faure, G. and Mensing, T.M. 1989*a*. The geochemistry of Jurassic dolerites from Portal Peak, Antarctica. *Contributions to Mineralogy and Petrology*, **102**, 298–305, https://doi.org/10.1007/BF00373722

Hergt, J.M., Chappell, B.W., McCulloch, T.M., McDougall, I. and Chivas, A.R. 1989*b*. Geochemical and isotopic constraints on the origin of the Jurassic dolerites of Tasmania. *Journal of Petrology*, **30**, 841–883, https://doi.org/10.1093/petrology/30.4.841

Hergt, J.M., Peate, D.W. and Hawksworth, C.J. 1991. The petrogenesis of Mesozoic Gondwana low-Ti flood basalts. *Earth and*

Planetary Science Letters, **105**, 134–148, https://doi.org/10.1016/0012-821X(91)90126-3

Hersum, G.T., Marsh, B.D. and Simon, C.A. 2007. Contact partial melting of granitic country rock, melt segregation, and re-injection as dikes into Ferrar Dolerite Sills, McMurdo Dry Valleys, Antarctica. *Journal of Petrology*, **48**, 2125–2148, https://doi.org/10.1093/petrology/egm054

Hildreth, W. and Moorbath, S. 1988. Crustal contributions to arc magmatism in the Andes of central Chile. *Contributions to Mineralogy and Petrology*, **98**, 455–489, https://doi.org/10.1007/BF00372365

Himmelberg, G.R. and Ford, A.B. 1976. Pyroxenes of the Dufek intrusion. *Journal of Petrology*, **17**, 219–243, https://doi.org/10.1093/petrology/17.2.219

Himmelberg, G.R. and Ford, A.B. 1977. Iron–titanium oxides of the Dufek intrusion. *American Mineralogist*, **62**, 623–633

Hoefs, J., Faure, G. and Elliot, D.H. 1980. Correlation of δ^{18}O and initial ^{87}Sr/^{86}Sr ratios in Kirkpatrick Basalt on Mt. Falla, Transantarctic Mountains. *Contributions to Mineralogy and Petrology*, **75**, 199–203, https://doi.org/10.1007/BF01166760

Hornig, I. 1993. High-Ti and low-Ti tholeiites in the Jurassic Ferrar Group, Antarctica. *Geologisches Jahrbuch*, **E47**, 335–369.

Hunter, S.J., Johnson, A.C. and Aleshkova, N.D. 1996. Aeromagnetic data from the southern Weddell Sea embayment and adjacent areas: synthesis and interpretation. *Geological Society, London, Special Publications*, **108**, 143–154, https://doi.org/10.1144/GSL.SP.1996.108.01.10

Isaac, M.J., Chinn, T.J., Edbrooke, S.W. and Forsyth, P.J. 1996. *Geology of the Olympus Range Area, Southern Victoria Land, Antarctica, Scale 1:50 000*. Institute of Geological and Nuclear Sciences Geological Map, **20**.

Ishii, T. 1975. The relations between temperature and composition of pigeonite in some lavas and their application to geothermometry. *Mineralogical Journal*, **8**, 48–57, https://doi.org/10.2465/minerj.8.48

Ivanov, A.V., Meffre, S., Thompson, J., Corfu, F., Kamenetsky, V.S., Kamenetsky, M.B. and Demonterova, E.I. 2017. Timing and genesis of the Karoo–Ferrar large igneous province: New high precision U–Pb data for Tasmania confirm short duration of the major magmatic pulse. *Chemical Geology*, **455**, 32–43, https://doi.org/10.1016/j.chemgeo.2016.10.008

Jerram, D.A., Davis, G.R., Mock, A., Charrier, A. and Marsh, B.D. 2010. Quantifying 3D crystal populations, packing and layering in shallow intrusions: A case study from the Basement Sill, Dry Valleys, Antarctica. *Geosphere*, **6**, 537–548, https://doi.org/10.1130/GES00538.1

Jordan, T.A., Ferraccioli, F. and Leat, P.T. 2017. New geophysical compilations link crustal block motion to Jurassic extension and strike-slip faulting in the Weddell Sea Rift System of West Antarctica. *Gondwana Research*, **42**, 29–48, https://doi.org/10.1016/j.gr.2016.09.009

Jourdan, F., Bertrand, H., Schörer, U., Blichert-Toft, J., Féraud, G. and Kampunzu, A.B. 2007. Major and trace element and Sr, Nd, Hf, and Pb isotope compositions of the Karoo Large Igneous Province, Botswana–Zimbabwe: lithosphere vs mantle plume combination. *Journal of Petrology*, **48**, 1043–1077, https://doi.org/10.1093/petrology/egm010

Kistler, R.W., White, L.D. and Ford, A.B. 2000. *Strontium and Oxygen Isotopic Data and Age for the Layered Gabbroic Dufek Intrusion, Antarctica*. United States Geological Survey Open-File Report, **00-133**.

Kyle, P.R. 1980. Development of heterogeneities in the subcontinental mantle: evidence from the Ferrar Group, Antarctica. *Contributions to Mineralogy and Petrology*, **73**, 89–104, https://doi.org/10.1007/BF00376262

Kyle, P.R., Pankhurst, R.J. and Bowman, J.R. 1983. Isotopic and chemical variations in Kirkpatrick Basalt Group rocks from southern Victoria Land. *In*: Oliver, R.L., James, P.R. and Jago, J.B. (eds) *Antarctic Earth Science*. Australian Academy of Science, Canberra, 234–237.

Kyle, P.R., Pankhurst, R.J., Bowman, J.R., Millar, I.L. and McGibbon, R. 1987. Enriched subcontinental lithospheric mantle along the Pacific margin of Gondwana: isotopic studies of Jurassic Ferrar Supergroup tholeiites. *In*: *Abstracts of the Fifth International Symposium on Antarctic Earth Sciences, Cambridge, August 1987*. Cambridge University Press, Cambridge, UK, 86.

Kyle, P.R., Pankhurst, R.J., Esser, R. and Shelhorn, M.A. 1999. Petrogenesis of the Jurassic Butcher Ridge Igensous Complex, Ferrar Large Igneous Province, Antarctica. *In*: *Proceedings of the 8th International symposium on Antarctic Earth Sciences, 5–9 July, 1999, Wellington, New Zealand, Programme and Abstracts*. Royal Society of New Zealand, Wellington, 178.

Lanza, R and Zanella, E. 1993. Paleomagnetism of the Ferrar dolerite in the northern Prince Albert Mountains (Victoria Land, Antarctica). *Geophysical Journal International*, **114**, 501–511, https://doi.org/10.1111/j.1365-246X.1993.tb06983.x

Leat, P.T. 2008. On the long-distance transport of Ferrar magmas. *Geological Society, London, Special Publications*, **302**, 45–61, https://doi.org/10.1144/SP302.4

Leat, P.T., Riley, T.R., Storey, B.C., Kelley, S.P. and Millar, I.L. 2000. Middle Jurassic ultramafic lamprophyre dyke within the Ferrar magmatic province, Pensacola Mountains, Antarctica. *Mineralogical Magazine*, **64**, 95–111, https://doi.org/10.1180/002646100549021

Leat, P.T., Dean, A.A., Millar, I.L., Kelley, S.P., Vaughan, A.P.M. and Riley, T.R. 2005. Lithospheric mantle domains beneath Antarctica. *Geological Society, London, Special Publications*, **246**, 359–380, https://doi.org/10.1144/GSL.SP.2005.246.01.15

Leat, P.T., Luttinen, A.V., Storey, B.C. and Millar, I.L. 2006. Sills of the Theron Mountains, Antarctica: evidence for long distance transport of mafic magmas during Gondwana break-up. *In*: Hanski, E., Mertanen, S., Rämö, T. and Vuollo, J. (eds) *Dyke Swarms: Markers of Crustal Evolution*. Taylor and Francis, Abingdon, UK, 183–199.

Lindsley, D.H. 1983. Pyroxene thermometry. *American Mineralogist*, **68**, 447–493.

Lindsley, D.H. and Andersen, D.J. 1983. A two-pyroxene thermometer. *Journal of Geophysical Research: Solid Earth*, **88**(S02), A887–A905, https://doi.org/10.1029/JB088iS02p0A887

Lisker, F. and Läufer, A.L. 2013. The Mesozoic Victoria Basin: Vanished link between Antarctica and Australia. *Geology*, **41**, 1043–1046, https://doi.org/10.1130/G33409.1

Loewy, S.L., Dalziel, I.W.D., Pisarevsky, S., Connelly, J.N., Tait, J., Hanson, R.E. and Bullen, D. 2011. Coats Land crustal block, East Antarctica: A tectonic tracer for Laurentia? *Geology*, **39**, 859–862, https://doi.org/10.1130/G32029.1

Magee, C., Muirhead, J.D. *et al*. 2016. Lateral flow in mafic sill complexes. *Geosphere*, **12**, 809–841, https://doi.org/10.1130/GES01256.1

Magee, C., Ernst, R.E., Muirhead, J.D., Phillips, T. and Jackson, C.A.L. 2019. Magma transport pathways in large igneous provinces: lessons from combining field observations and seismic reflection data. *In*: Srivastava, R.K., Ernst, R.E. and Peng, P. (eds) *Dyke Swarms of the World: A Modern Perspective*. Springer, 45–85, https://doi.org/10.1007/978-981-13-1666-1_2

Marsh, B.D. 1998. On the interpretation of crystal size distributions in magmatic systems. *Journal of Petrology*, **39**, 553–599, https://doi.org/10.1093/petroj/39.4.553

Marsh, D.B. 2004. A magmatic mush column Rosetta Stone: The McMurdo Dry Valleys of Antarctica. *Eos, Transactions of the American Geophysical Union*, **86**, 497–502, https://doi.org/10.1029/2004EO470001

Marsh, B D. 2007. Magmatism, magma, and magma chambers. *Treatise on Geophysics*, **6**, 273–323, https://doi.org/10.1016/B978-0-444-53802-4.00116-0

Marsh, D.B. and Zieg, M.J. 1997. The Dais layered intrusion: a new discovery in the Basement Sill of the McMurdo Dry Valleys. *Antarctic Journal of the United States*, **32**, 18–20.

Marsh, B.D., Hersum, T.G., Simon, A.C., Charrier, A.D. and Souter, B.J. 2005. Discovery of a funnel-like deep feeder zone for the Ferrar Dolerites, McMurdo Dry Valleys, Antarctica. *Eos, Transactions of American Geophysical Union*, **86**(52), Fall Meeting Supplement, abstract V14C-03.

Marsh, J.S., Hooper, P.R., Rehacek, J., Duncan, R.A. and Duncan, A.R. 1997. Stratigraphy and age of Karoo basalts of Lesotho and implications for correlations within the Karoo igneous province. *American Geophysical Union Geophysical Monograph Series*, **100**, 247–272.

Marshak, S., Kyle, P.R., McIntosh, W., Samsonov, V. and Shellhorn, M. 1981. Butcher Ridge igneous complex, Cook Mountains, Antarctica. *Antarctic Journal of the United States*, **16**, 54–55.

McElroy, C.T. and Rose, G. 1987. *Geology of the Beacon Heights Area, Southern Victoria Land, Antarctica, Scale 1:50 000*. New Zealand Geological Survey Miscellaneous Series Map, **15**.

McIntosh, W.C., Kyle, P.R. and Sutter, J.F. 1986. Paleomagnetic results from the Kirkpatrick Basalt group, Mesa Range, north Victoria Land, Antarctica. *American Geophysical Union Antarctic Research Series*, **46**, 289–303.

McLelland, D. 1967. *Geology of the Basement Complex, Thorvald Nilsen Mountains, Antarctica*. MS thesis, University of Nevada, Reno, Nevada, USA.

Melluso, L., Hergt, J.M. and Zanetti, A. 2014. The late crystallization stages of low-Ti, low-Fe tholeiitic magmas; insights from evolved Antarctic and Tasmanian rocks. *Lithos*, **188**, 72–83, https://doi.org/10.1016/j.lithos.2013.10.032

Mensing, T.M. and Faure, G. 1996. Cretaceous alteration of Jurassic volcanic rocks, Pain Mesa, northern Victoria Land, Antarctica. *Chemical Geology*, **129**, 153–161, https://doi.org/10.1016/0009-2541(95)00155-7

Mensing, T.M., Faure, G., Jones, L.M., Bowman, J.R. and Hoefs, J. 1984. Petrogenesis of the Kirkpatrick Basalt, Solo Nunatak, north Victoria Land, Antarctica. *Contributions to Mineralogy and Petrology*, **87**, 101–108, https://doi.org/10.1007/BF00376216

Mensing, T.M., Faure, G., Jones, L.M. and Hoefs, J. 1991. Stratigraphic correlation and magma evolution of the Kirkpatrick Basalt in the Mesa Range, northern Victoria Land, Antarctica. *In*: Ulbrich, H. and Rocha Campos, A.C. (eds) *Gondwana Seven Proceedings. Papers presented at the Seventh International Gondwana Symposium, Sao Paulo, 1988*. Institut Geociências, Universidade de São Paulo, São Paulo, Brazil, 653–667.

Menzies, M.A. and Kyle, P.R. 1990. Continental volcanism: a crust–mantle probe. *Oxford Monographs on Geology and Geophysics*, **16**, 157–177.

Milnes, A.R., Cooper, B.J. and Cooper, J.A. 1982. The Jurassic Wisanger basalt of Kangaroo Island, South Australia. *Royal Society of South Australia Transactions*, **106**, 1–13.

Molzahn, M., Reisberg, L. and Wörner, G. 1996. Os, Sr, Nd, Pb, O isotope and trace element data from the Ferrar flood basalts, Antarctica: evidence for an enriched subcontinental lithospheric source. *Earth and Planetary Science Letters*, **144**, 529–546, https://doi.org/10.1016/S0012-821X(96)00178-1

Molzahn, M., Wörner, G., Henjes-Kunst, F. and Rocholl, A. 1999. Constraints on the Cretaceous thermal event in the Transantarctic Mountains from alteration processes in Ferrar flood basalts. *Global and Planetary Change*, **23**, 45–60, https://doi.org/10.1016/S0921-8181(99)00050-8

Morrison, A.D. and Reay, A. 1995. Geochemistry of Ferrar Dolerite sills and dykes at Terra Cotta Mountains, south Victoria Land, Antarctica. *Antarctic Science*, **7**, 73–85, https://doi.org/10.1017/S0954102095000113

Mortimer, N., Parkinson, D., Raine, J.I., Adams, C.J., Graham, I.J., Oliver, P.J. and Palmer, K. 1995. Ferrar magmatic province rocks discovered in New Zealand: Implications for Mesozoic Gondwana geology. *Geology*, **23**, 185–188, https://doi.org/10.1130/0091-7613(1995)023<0185:FMPRDI>2.3.CO;2

Muirhead, J.D., Airoldi, J., Rowland, J.V. and White, J.D.L. 2012. Interconnected sills and inclined sheet intrusions control shallow magma transport in the Ferrar large igneous province, Antarctica. *Bulletin of the Geological Society of America*, **124**, 162–180, https://doi.org/10.1130/B30455.1

Mukasa, S.B., Andronikov, A.V. and Carlson, R.W. 2003. Myth of the Dufek Plume: Nd, Sr, Pb and Os isotopic and trace element data in support of a subduction origin. *In*: *9th International Symposium on Antarctic Earth Sciences, Potsdam, Germany, 8–12 September 2003*. Programme and Abstracts. Terra Nostra, Potsdam, Germany, 238.

Mukasa, S.B., Ravizza, G., Bédard, J., Choi, S., Andronikov, A.V. and Fleming, T.H. 2007. Dufek layered mafic intrusion and Basement Sill, Antarctica: constraints on their magma sources based on PGE abundance patterns, Nd–Sr–Pb isotopic ratios and trace element modeling. *Eos Transactions of the American Geophysical Union*, **88**(52), Fall Meeting Supplement, abstract V53D-03.

Nelson, D.A. and Cottle, J.M. 2016. Formation of layering in a hypabyssal intrusion by shear-induced fracture, exsolution, and rapid devitrification. *Goldschmidt Conference Abstracts*, **2016**. 2262.

Nelson, D.A., Cottle, J.M., Barboni, M. and Schoene, B. 2014. Petrologic significance of silicic magmatism in the Ferrar Large Igneous Province: geochemistry and geochronology of the Butcher Ridge Igneous Complex, Antarctica. *Eos, Transactions of the American Geophysical Union*, Fall Meeting 2014, **95**, abstract V33A-4831.

Nelson, D.A., Cottle, J.M. and Bindeman, I. 2018. Jurassic volcanic glass in the Ferrar large Igneous Province of Antarctica preserves evidence for hydration by glacial meltwater. *Eos, Transactions of the American Geophysical Union*, Fall Meeting 2018, **99**, abstract V23J-0182.

Neumann, E.R., Svensen, H., Galerne, C.Y. and Planke, S. 2011. Multistage evolution of dolerites in the Karoo large igneous province, central South Africa. *Journal of Petrology*, **52**, 959–984, https://doi.org/10.1093/petrology/egr011

Petford, N. and Mirhadizadeh, S. 2017. Image-based modelling of lateral flow: the Basement Sill, Antarctica. *Royal Society Open Science*, **4**, 161083, https://doi.org/10.1098/rsos.161083

Pocknall, D.T., Chinn, T.J., Sykes, R. and Skinner, D.N.B. 1994. *Geology of the Convoy Range Area, Southern Victoria Land, Antarctica, Scale 1:50 000*. Institute of Geological and Nuclear Sciences Geological Map, **11**.

Prior, G.T. 1907. Report on the rock specimens collected during the 'Discovery' Antarctic Expedition, 1901–1904. *National Antarctic Expedition 1901–1904, Natural History, Geology (Field Geology, Petrography)*, **1**, 101–140.

Ramirez, C., Nyblade, A. *et al*. 2017. Crustal structure of the Transantarctic Mountains, Ellsworth Mountains and Marie Byrd Land, Antarctica: constraints on shear wave velocities, Poisson's ratios and Moho depths. *Geophysical Journal International*, **211**, 1328–1340, https://doi.org/10.1093/gji/ggx333

Ricker, J. 1964. Outline of the geology between the Mawson and Priestley Glaciers, Victoria Land. *In*: Adie, R.J. (ed.) *Antarctic Geology*. North-Holland, Amsterdam, 265–275.

Riley, T.R., Curtis, M.L., Leat, P.T., Watkeys, M.K., Duncan, R.A., Millar, I.L. and Owens, W.H. 2006. Overlap of Karoo and Ferrar magma types in KwaZulu–Natal, South Africa. *Journal of Petrology*, **47**, 541–566, https://doi.org/10.1093/petrology/egi085

Riley, J.R., Taylor, B.M. and Fleming, T.H. 2020. Geochemistry of Jurassic Dolerite Intrusions in the Ohio Range and Southern Queen Maud Mountains, Antarctica. *Geological Society of America Abstracts with Programs*, **52**(2), https://doi.org/10.1130/abs/2020SE-345188

Roland, N.W. and Tessensohn, F. 1987. Rennick faulting – An early phase of Ross Sea rifting. *Geologisches Jahrbuch*, **66B**, 203–229.

Ross, P.-S., White, J.D.L. and McClintock, M.K. 2008. Physical volcanology of mafic volcaniclastic deposits and lavas in the Coombs–Allan Hills area, Ferrar large igneous province, Antarctica. *Journal of Volcanology and Geothermal Research*, **172**, 38–60, https://doi.org/10.1016/j.jvolgeores.2005.11.011

Rudnick, R.L. and Gao, S. 2003. Composition of the continental crust. *Treatise on Geochemistry*, **3**, 1–64.

Sarbas, B., Jochum, K.P., Nohl, U. and Weis, U. 2017. The geochemical databases GEOROC and GeoReM – what's new? *Eos, Transactions of the American Geophysical Union*, Fall Meeting 2017, **98**, abstract V23D-2629.

Sell, B., Ovtcharova, M. *et al*. 2014. Evaluating the temporal link between the Karoo LIP and climatic–biologic events of the Toarcian Stage with high-precision U–Pb geochronology. *Earth and Planetary Science Letters*, **408**, 48–56, https://doi.org/10.1016/j.epsl.2014.10.008

Semenov, V.S., Mikhailov, V.M., Koptev-Dvornikov, E.V., Ford, A.B., Shulyatin, O.G., Semenov, S.V. and Tkacheva, D.A. 2014. Layered Jurassic intrusions in Antarctica. *Petrology*, **22**, 547–573, https://doi.org/10.1134/S0869591114060034 (original Russian text in *Petrologiya*, 2014, **22**(6), 592–619).

Shellhorn, M.A. 1982. *The Role of Crustal Contamination at the Butcher Ridge Igneous Complex, Antarctica*. MS thesis, New Mexico Institute of Mining and Technology, Socorro, New Mexico, USA.

Sheth, H. 2018. *A Photographic Atlas of Flood Basalt Volcanism*. Springer, Berlin.

Siddoway, C.S. 2007. Tectonics of the West Antarctic Rift System: New light on the history and dynamics of distributed intracontinental extension. *United States Geological Survey Open-File Report*, **2007-1047**, 91–114.

Siders, M.A. and. Elliot, D.H. 1985. Major and trace element geochemistry of the Kirkpatrick Basalt, Mesa Range, Antarctica. *Earth and Planetary Science Letters*, **72**, 54–64, https://doi.org/10.1016/0012-821X(85)90116-5

Skinner, D.N.B. and Ricker, J. 1968. The geology of the region between the Mawson and Priestley Glaciers, north Victoria Land. *New Zealand Journal of Geology and Geophysics*, **11**, 1041–1075, https://doi.org/10.1080/00288306.1968.10420768

Souter, B.J., Marsh, B., Malolepszy, Z. and Morin, P. 2006. 3D structure of the feeder zone of the McMurdo Dry valleys magmatic system, Antarctica. *Eos, Transactions of the American Geophysical Union*, **87**(36), Joint Assembly Supplement, abstract V41A-21.

Spaeth, G., Hotten, R., Peters, M. and Techmer, K. 1995. Mafic dykes in the Shackleton range, Antarctica. *Polarforschung*, **63**, 101–121.

Stephenson, P.J. 1966. Geology 1: Theron Mountains, Shackleton Range and Whichaway Nunataks. *Trans-Antarctic Expedition, 1955–1958. Scientific Reports*, **8**.

Stewart, D. 1934. The petrography of some Antarctic rocks. *American Mineralogist*, **19**, 150–160.

Storey, B.C. and Alabaster, T. 1991. Tectonomagmatic controls on Gondwana breakup models: evidence from the proto-Pacific margin of Antarctica. *Tectonics*, **10**, 1274–1288, https://doi.org/10.1029/91TC01122

Storey, B.C. and Kyle, P R. 1997. An active mantle mechanism for Gondwana break-up. *South African Journal of Geology*, **100**, 283–290.

Studinger, M., Bell, R.E., Blankenship, D.D., Buck, W.R. and Karner, G.D. 2004. Sub-ice geology inland of the Transantarctic Mountains in light of new aerogeophysical data. *Earth and Planetary Science Letters*, **220,** 391–408, https://doi.org/10.1016/S0012-821X(04)00066-4

Studinger, M., Bell, R.E., Fitzgerald, P.G. and Buck, W.R. 2006. Crustal architecture of the Transantarctic Mountains between the Scott and Reedy Glacier region and the South Pole from aerogeophysical data. *Earth and Planetary Science Letters*, **250**, 182–199, https://doi.org/10.1016/j.epsl.2006.07.035

Sun, S-s. and McDonough, W.F. 1989. Chemical and isotopic systematics of oceanic basalts: implications for mantle composition and processes. *Geological Society, London, Special Publications*, **42**, 313–345, https://doi.org/10.1144/GSL.SP.1989.042.01.19

Svensen, H., Corfu, F., Polteau, S., Hammer, Ø. and Planke, S. 2012. Rapid magma emplacement in the Karoo Large Igneous Province. *Earth and Planetary Science Letters*, **325–326**, 1–9, https://doi.org/10.1016/j.epsl.2012.01.015

Tinto, K.J., Padman, L. *et al*. 2019. Ross Ice Shelf response to climate driven by the tectonic imprint on seafloor bathymetry. *Nature Geoscience*, **12**, 441–449, https://doi.org/10.1038/s41561-019-0370-2

Turnbull, I.M., Allibone, A.H., Forsyth, P.J. and Heron, D.W. 1994. *Geology of the Bull Pass–St Johns Range Area, Southern Victoria Land, Antarctica, Scale 1:50 000*. Institute of Geological and Nuclear Sciences Geological Map, **14**.

Veevers, J.J., Conaghan, P.J. and Powell, C.McA. 1994. Eastern Australia. *Geological Society of America Memoirs*, **184**, 11–171.

Vennum, W.R. and Storey, B.C. 1987. Correlation of gabbroic and diabasic rocks from the Ellsworth Mountains, Hart Hills, and Thiel Mountains, West Antarctica. *American Geophysical Union Geophysical Monograph Series*, **40**, 129–138.

Wilhelm, S. and Wörner, G. 1996. Crystal size distribution in Jurassic Ferrar flows and sills (Victoria Land, Antarctica): evidence for processes of cooling, nucleation and crystallization. *Contributions to Mineralogy and Petrology*, **125**, 1–15, https://doi.org/10.1007/s004100050202

Will, T.M., Frimmel, H.E., Zeh, A., Le Roux, P. and Schmädicke, E. 2010. Geochemical and isotopic constraints on the tectonic and crustal evolution of the Shackleton Range, East Antarctica, and correlation with other Gondwana crustal segments. *Precambrian Research*, **180**, 85–112, https://doi.org/10.1016/j.precamres.2010.03.005

Woolfe, K.J., Kirk, P.A. and Sherwood, A.M. 1989. *Geology of the Knobhead Area, Southern Victoria Land, Antarctica, Scale 1:50 000*. New Zealand Geological Survey Miscellaneous Series Map, **19**.

Zavala, K., Leitch, A.M. and Fisher, G.W. 2011. Silicic segregations of the Ferrar Dolerite sills, Antarctica. *Journal of Petrology*, **52**, 1927–1964, https://doi.org/10.1093/petrology/egr035

Zieg, M.J. and Marsh, D.B. 2012. Multiple reinjections and crystal-mush compaction in the Beacon sill, McMurdo Dry Valleys, Antarctica. *Journal of Petrology*, **53**, 2567–2591, https://doi.org/10.1093/petrology/egs059